Abstract

THAMES, MURRAY CAMERON. Application and Assessment of a 9-equation Subchannel Methodology to Rod Bundles. (Under the direction of Dr. J. Michael Doster).

The 9-equation subchannel methodology found in COBRA-TF (CTF) has been evaluated against data from subcooled boiling experiments. COBRA-TF employs mass, energy and momentum conservation equations for three separate flow fields (liquid, vapor and entrainment). Experiments consisting of 5x5 and 4x4 rod bundle geometries were simulated. Test cases allowed for comparison of void fraction, flow quality, enthalpy, and temperature to experimental values. In addition, a 17x17 model of a standard pressurized water reactor fuel assembly was constructed in order to assess turbulent mixing models and heat conduction options found in CTF. It was found that the heat transfer models in CTF were inappropriate for simulations of subcooled boiling conditions. In addition, while the code was able to predict bundle average properties with reasonable accuracy, significant differences were observed between the experimental and computed exit fluid temperature and mass flux for individual subchannels. Recommendations were made that may improve the accuracy of the code for subcooled boiling conditions. Further assessments of COBRATF need to be made in order to validate its performance in more robust boiling regimes and to correct other issues found in this study.

Application and Assessment of a 9-equation Subchannel Methodology to Rod Bundles

by

Murray Cameron Thames

A thesis submitted to the Graduate Faculty of
North Carolina State University in
partial fulfillment of the
requirements for the degree of
Master of Science

Nuclear Engineering

Raleigh, North Carolina

2014

APPROVED BY:

_____	_____
Dr. Hong Luo	Dr. Nam Dinh

_____

Dr. J. Michael Doster
Chair of Advisory Committee

Biography

Murray Cameron Thames was born in Winston Salem, NC in 1990. He enrolled in North Carolina State University's Nuclear Engineering program in the fall of 2008. After obtaining a Bachelor's degree in Nuclear Engineering, he stayed to pursue a Master's degree under the direction of Dr. J. Michael Doster. His work deals in Reactor Thermal-Hydraulics, with an emphasis on Subchannel methods. He completed his Master's degree in 2014.

Acknowledgements

I would like to thank Dr. J. Michael Doster for imparting invaluable knowledge on subchannel methods and for his guidance through the duration of this project.

Table of Contents

List of Tables

List of Figures

1. Introduction

1.1 Overview:

The subchannel equations are a pseudo three-dimensional set of conservation equations that may be utilized to evaluate flow conditions in multiple "channels" along a set flow direction. The conserved properties are mass, energy and momentum for each phase present (liquid, vapor, etc.). These equations may be used to determine thermal hydraulic properties in nuclear reactor rod bundles. A specific formulation of the subchannel equations for reactor purposes is the 9-equation model found in COBRA-TF (CTF) [1]. This methodology solves fluid conservation equations for a liquid, vapor and entrainment phase. This is a rigorous approach to obtaining the flow solution since the three equation sets are coupled, thus the solution for each quantity of interest must be obtained at each spatial location. This increases the computational requirements, but may assure a more accurate solution. Other methodologies allow the equation sets to be combined, providing conservation equations for the fluid mixture as a whole. To account for the loss of information from the equation reduction, additional correlations are used that relate phasic properties to the associated mixture properties. These "mixture" equations are less computationally expensive however, since the mixture equations rely on empirical correlations to obtain phasic quantities, the resulting solution may be less accurate. Two mixture equation formulations are available in COBRA-EN [2]. The three-equation model utilizes the three mixture equations that track the mass, energy and momentum of the fluid mixture. The four-equation model uses the three mixture equations in addition to a vapor mass conservation equation. The addition of the vapor conservation equation reduces the reliance on empirical correlations. In order to assess the capabilities of the methodology found in CTF a set of test cases were constructed based on physical experiments. The current focus in CTF development is to ensure that the code can accurately predict flow conditions under subcooled nucleate boiling. The conditions in the physical experiments ranged from single phase liquid to slightly saturated flow. The CTF numerical solution was compared to the physical data, with the quantities of interest being: flow quality, fluid temperature/enthalpy, void fraction, mass flux and wall temperature. To further assess the

CTF solution, additional comparisons were made based on the results obtained from the three and four equation models found in COBRA-EN.

1.2 Flow Conservation Equations

The subchannel equations obtain their name based on the control volume over which they are evaluated. In nuclear reactors, the control volume is restricted in the radial direction by the orientation and spacing of the rods. For a square lattice, the radial layout for a single subchannel would be viewed as:

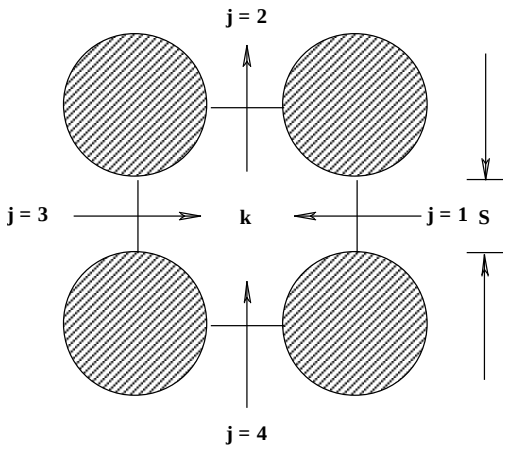

Figure 1-1: Subchannel for a square lattice

With a finite axial spacing specified, the control volume for this type of radial layout is shown in Figure 1-2.

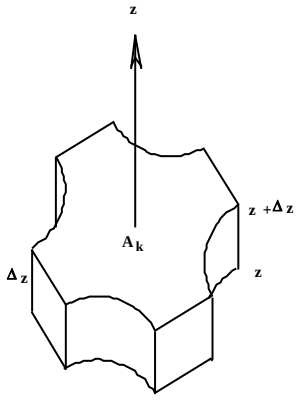

Figure 1-2: Control volume for subchannel

In the case of a nuclear reactor, the spatial region between the fuel rods will be discretized into these control volumes. Near the periphery of the core/fuel bundle, the control volume will be reduced due to the flow area restriction imposed from the boundary.

The equations that are evaluated over the control volume ensure conservation of mass, energy and momentum. For any phase, k, the conservations equations are given by:

Mass:

$$\frac{\partial}{\partial t}(\alpha_k \rho_k) + \frac{\partial}{\partial x}(\alpha_k \rho_k u_k) + \sum_{j=1}^{nchannel}(\alpha_k \rho_k w_k)_j = L_k + \sum_{j=1}^{nchannel}(M_k^{'''})_j \tag{1.1}$$

Axial Momentum:

$$\frac{\partial}{\partial t}(\alpha_k \rho_k u_k) + \frac{\partial}{\partial x}(\alpha_k \rho_k u_k u_k) + \sum_{j=1}^{nchannel}(\alpha_k \rho_k u_k w_k)_j = \tag{1.2}$$
$$-\alpha_k \frac{\partial P}{\partial x} - \alpha_k \rho_k g + \mathrm{M}_k^{du} + M_k^{Lu} + \sum_{j=1}^{nchannel}(M_k^{T'''})_j$$

Lateral Momentum:

$$\frac{\partial}{\partial t}(\alpha_k \rho_k w_k) + \frac{\partial}{\partial z}(\alpha_k \rho_k w_k w_k) + \frac{\partial}{\partial x}(\alpha_k \rho_k w_k u_k) = -\alpha_k \frac{\partial P}{\partial z} + \mathrm{M}_k^{dw} + M_k^{Lw} \tag{1.3}$$

Vapor Energy :

$$\frac{\partial}{\partial \mathrm{t}}(\alpha_v \rho_v h_v) + \frac{\partial}{\partial \mathrm{x}}(\alpha_v \rho_v h_v u_v) + \sum_{j=1}^{nchannel}(\alpha_v \rho_v h_v w_v)_j = \tag{1.4}$$
$$-\sum_{j=1}^{nchannel} q_v^{T'''} + \Gamma''' h + q_{wv}''' + \alpha_v \frac{\partial P}{\partial t}$$

Liquid Energy :

$$\frac{\partial}{\partial \mathrm{t}}(\alpha_l \rho_l h_l) + \frac{\partial}{\partial \mathrm{x}}(\alpha_l \rho_l h_l u_l) + \frac{\partial}{\partial \mathrm{x}}(\alpha_e \rho_e h_e u_e) + \sum_{j=1}^{nchannel}(\alpha_l \rho_l h_l w_l)_j + \sum_{j=1}^{nchannel}(\alpha_e \rho_e h_e w_e)_j = \tag{1.5}$$
$$-\sum_{j=1}^{nchannel} q_l^{T'''} - \Gamma''' h + q_{wl}''' + (\alpha_l + \alpha_e)\frac{\partial P}{\partial t}$$

These equations yield time-dependent conservation of the liquid, vapor and entrainment (droplet) fields. The flow is modeled in the principal axial direction via equations 1.1, 1.2, 1.4 and 1.5. It should be noted that the advection of the liquid and entrainment energy is modeled in one equation. These equations take on a similar form, each conserving the specific quantity according to an advection process. The source terms on the right-hand side are produced from: the interactions of the current phase with other phases, interactions with physical boundaries (rod walls), transfer from an adjacent channel or a pressure difference. In order to accurately obtain the transfer of the conserved quantities between channels, an additional lateral momentum equation is required. Equation 1.3 ensures this through a similar advection equation that is driven through a lateral pressure gradient and phase change.

When considering the interaction of phases with other phases or physical boundaries, it is important to specify what each source term entails. The L_k term shown in equation 1.1 is the source term incurred from mass transfer into or out of phase k. This mass transfer may occur either from evaporation/condensation or entrainment/de-entrainment. The second source term in the mass conservation equation represents mass transfer that occurs through turbulent mixing and void drift from adjacent subchannels. The first two source terms shown in the axial momentum equation represent the acceleration of the flow due to a pressure differential and the presence of gravity. The third source term takes into account the effects of interfacial drag in the axial direction. For the three given fields, this term may be expanded as:

$$M_v^{du} = -\tau_{i,vl}''' - \tau_{i,ve}''' \quad (1.6)$$

$$M_l^{du} = \tau_{i,vl}''' \quad (1.7)$$

$$M_e^{du} = \tau_{i,ve}''' \quad (1.8)$$

Each term in equations 1.6, 1.7 and 1.8 represent a volumetric interfacial drag force that occurs from interaction of the current phase with the remaining phases. The notation that

CTF uses assumes that liquid and entrainment produce a force on the vapor in the negative principle flow direction. This is the exact same force that occurs as a source term for the liquid and entrainment phases, but now in the positive direction. The remaining two source terms in the axial momentum equation follow directly from the source terms found in the mass equation. M_k^{Lu} is the momentum transfer that occurs due to phase change, and the final summation term is the result of turbulent mixing and void drift from surrounding subchannels.

The remaining source terms pertain to energy conservation. The first summation source term represents the transmission of energy from turbulent mixing with adjacent channels. The second source term represents the addition or removal of enthalpy with phase change. The third source term is the effect of wall heat transfer to the vapor or liquid phase. Lastly, the final term indicates the phasic energy addition due to pump work.

The actual control volume used in the numerical evaluation of the conservation equations takes on a different geometry than that previously shown. With the specification of an axial discrete length, the control volume would resemble a rectangular prism. This can be viewed in Figure 1-3.

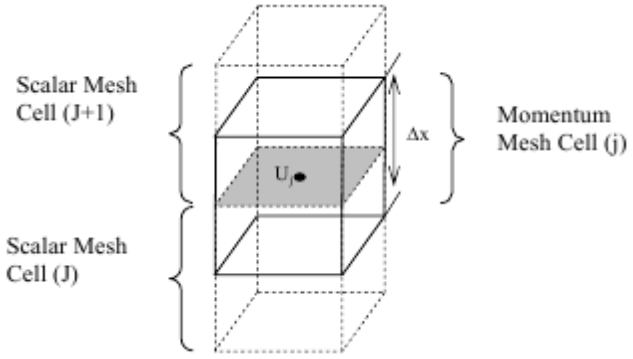

Figure 1-3: Axial subchannel mesh used in CTF

This layout allows for the solution of the conserved quantities, $\mathbf{U}_j$, evaluated at the cell-center. Additionally, when the lateral momentum equation is evaluated, the control volume will take on a similar shape:

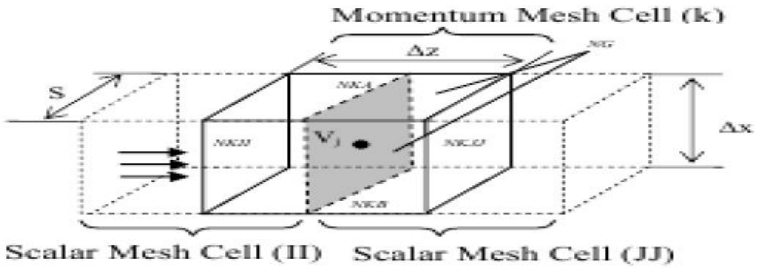

Figure 1-4: Lateral subchannel mesh used in CTF

With the meshing specified for a particular geometry, the time-dependent flow conservation equations may be solved numericall

2. Description of Test Cases

2.1 Castellana 4x4:

Four specific geometries were utilized when developing test cases for CTF. These geometries were taken from physical experiments performed by Castellana and Casterline [4], EPRI [3] and a standard 17x17 PWR fuel bundle [5]. The experimental set-up used by Castellana allowed for the evaluation of exit flow quantities within a 4x4 test assembly. The subchannel map for this assembly is shown in Figure 2-1.

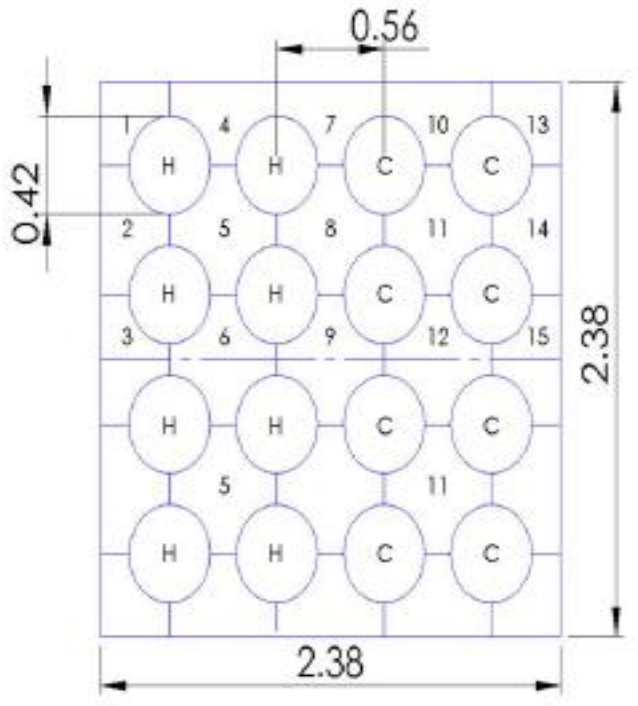

Figure 2-1: Castellana 4x4 Subchannel Map

The map displays 15 separate subchannels spanning half of the test assembly. A line of symmetry is shown splitting the assembly. This indicates a reflection of the rod powers about the lateral mid-plane. The power specification for each rod is labeled with either “H” or “C”, which represent a hot or cold rod respectively. The physical dimensions of the test assembly

are shown in Table 2-1. The radial peaking varies according to the ratio of the heat flux applied, while the profile is uniform along the total length.

Table 2-1: 4x4 Assembly Dimensions

Castellana 4x4:	
Rod Diameter:	0.422 in.
Rod Pitch:	0.555 in.
Rod-to-Wall Spacing:	0.148 in.
Ratio of Heat Flux:	
Hot Rods (H)	1.0
Cold Rods (C)	0.86
Heated Length:	60.0 in.
Assembly Dimensions:	2.383 in. x 2.383 in.

2.2 EPRI 5x5:

The remaining comparisons were taken from the data collected from the experimental setup utilized by EPRI. These tests allowed for the collection of exit flow quantities, as well as rod temperatures near the exit of the assembly. EPRI collected data for two separate 5x5 test assemblies (labeled assembly 74 and 75). A subchannel map for assembly 74 can be viewed in Figure 2-2. The differences between the two test assemblies comes from variation in the pitch in both lateral directions (x and y). These geometric differences are shown in Table 2-2. In addition, there are slight differences in the radial peaking factors, which are displayed explicitly in Table 2-3.

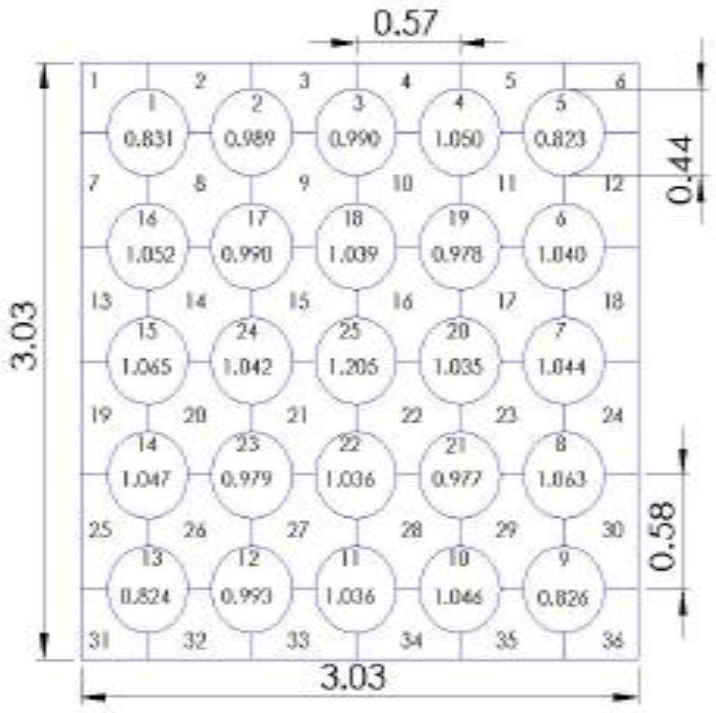

Figure 2-2: Assembly 74 subchannel map

Table 2-2: 5x5 Assembly Dimensions

EPRI 5x5:	Test 74	Test 75
Rod Diameter:	0.440 in.	0.440 in.
Rod Pitch (x):	0.566 in.	0.590 in.
Rod Pitch (y):	0.580 in.	0.580 in.
Rod-to-Wall Spacing (x):	0.142 in.	0.130 in.
Rod-to-Wall Spacing (y):	0.135 in.	0.135 in.
Heated Length:	84.0 in.	84.0 in.
Assembly Dimensions:	3.03 in. x 3.03 in.	3.03 in. x 3.03 in.

Table 2-3: 5x5 Rod Radial Peaking Factors

Rod #	Test 74	Test 75
1	0.831	0.834
2	0.989	0.993
3	0.99	0.994
4	1.05	1.055
5	0.823	0.826
6	1.04	1.045
7	1.044	1.047
8	1.063	1.058
9	0.826	0.827
10	1.046	1.048
11	1.036	1.026
12	0.993	0.989
13	0.824	0.826
14	1.047	1.055
15	1.065	1.06
16	1.052	1.054
17	0.99	0.997
18	1.039	1.03
19	0.978	0.983
20	1.035	1.031
21	0.977	0.981
22	1.036	1.025
23	0.979	0.984
24	1.042	1.03
25	1.205	1.201

In order to capture the wall temperatures near the exit of the assemblies, thermocouples were attached at four specific axial locations. One of the temperature measurements occurred before the final grid spacer, while the remaining three were taken above the spacer. A total of five spacer grids exist over the heated length. A diagram of the referenced axial locations is shown in Figure 2-3.

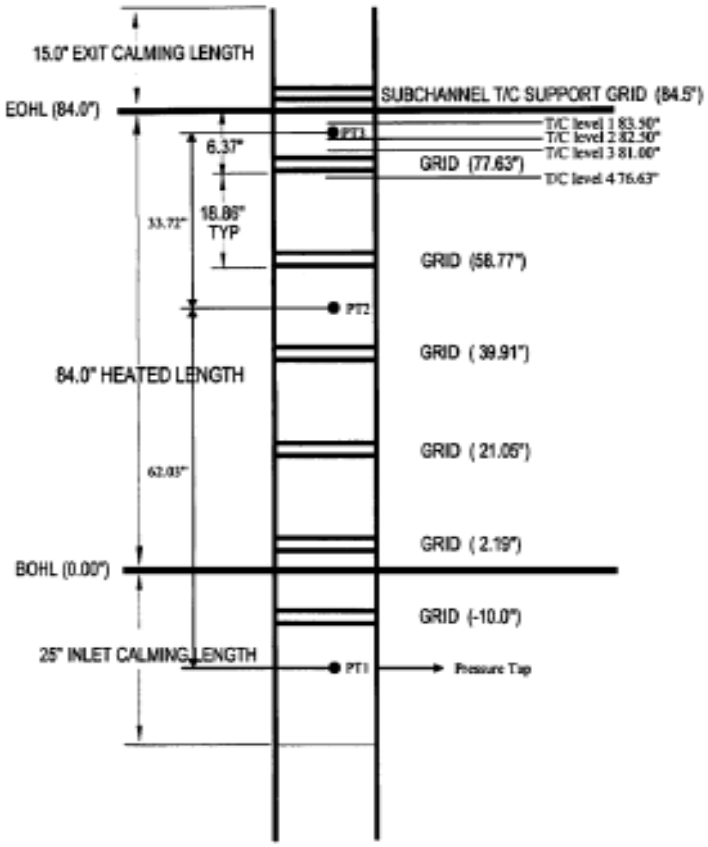

Figure 2-3: Grid and thermocouple configuration for 5x5 assembly

2.3 Standard 17x17:

The final set of numerical tests were performed on a typical 17x17 PWR bundle. While there was no physical data that could be used as a basis for comparison, these tests would provide a measure of the differences between CTF and COBRA-EN for a realistic problem. A quarter assembly model can be seen in Figure 2-4. In addition, rod peaking factors, a description of the geometry and flow conditions are shown in Tables 2-4, 2-5, 2-6 and 2-7. When the compete assembly geometry is considered, there are 25 water (unheated) rods and 264 heated rods.

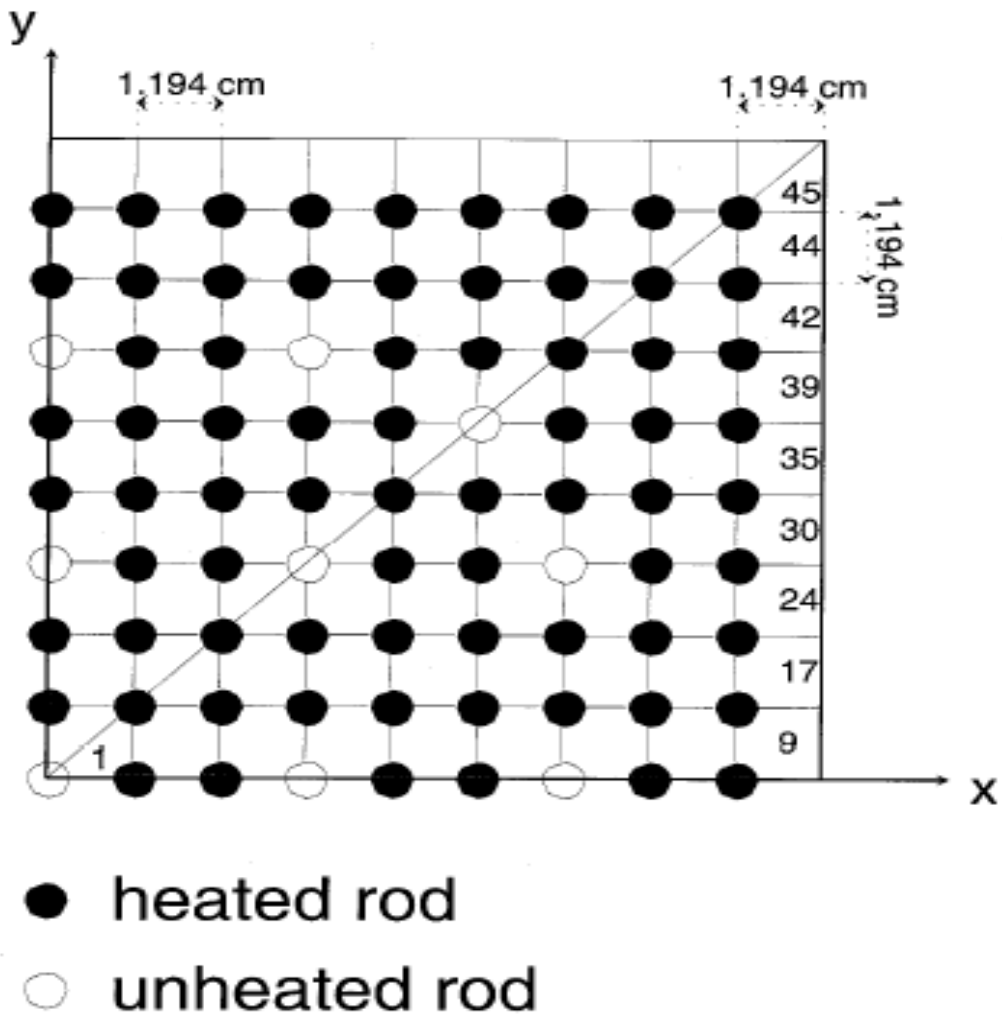

Figure 2-4: 17x17 quarter assembly

Table 2-4: 17x17 Axial peaking factors

Axial Position [ft]	Peaking Factor
0.000000	0.34490745
0.500000	0.51193255
0.833330	0.61983158
1.166660	0.72426432
1.500000	0.82464972
1.833320	0.92041756
2.166650	1.01104109
2.500000	1.09601551
2.833310	1.17485088
3.166640	1.24712105
3.500000	1.31242251
3.833300	1.37037344
4.166630	1.4206664
4.500000	1.46301916
4.833290	1.49718113
5.166620	1.52297502
5.500000	1.54025393
5.833280	1.5489154
6.166610	1.54891683
6.500000	1.54025393
6.833270	1.52298213
7.166600	1.49719103
7.500000	1.46301916
7.833260	1.4206817
8.166590	1.37039132
8.500000	1.31242251
8.833250	1.24714377
9.166580	1.17487583
9.500000	1.09601551
9.833240	1.01107009
10.166570	0.92044834
10.500000	0.82464972
10.833230	0.72429815
11.166560	0.61986664
11.500000	0.51193255
12.000000	0.34490745

Table 2-5: 17x17 Radial peaking factors for lower half of upper right quadrant

									1.04	**45**
								1.05	1.04	**44**
							1.1	1.07	1.04	**42**
						0	1.14	1.08	1.04	**39**
					1.17	1.18	1.16	1.1	1.05	**35**
				0	1.19	1.18	0	1.12	1.05	**30**
			1.17	1.19	1.17	1.16	1.16	1.1	1.05	**24**
		1.17	1.17	1.19	1.17	1.16	1.16	1.1	1.05	**17**
	0	1.2	1.2	0	1.19	1.18	0	1.12	1.05	**9**
Rod #:	**1**	**2**	**3**	**4**	**5**	**6**	**7**	**8**	**9**	

Table 2-6: 17x17 geometry parameters and flow conditions

17x17 Assembly Parameters	
Vertical Length (in):	167.992
Number of Fuel Rods:	264
Number of Water Rods:	25
Mass Flux (lbm/hr-ft^2):	2.7E+06
Inlet Enthalpy (Btu/lbm):	557
Rod Diameter (in):	0.374
Pitch (in):	0.4704
Pressure (psia):	2254
Flow Area (ft^2):	0.0349
Number of Grid Spacers:	8

Table 2-7: 17x17 Grid locations

Grid #	Initial Height (ft)	Final Height (ft)
1	0	0.12683727
2	2.012598425	2.137598425
3	3.72519685	3.85019685
4	5.437795276	5.562795276
5	7.150393701	7.275393701
6	8.862992126	8.987992126
7	10.57559055	10.70059055
8	11.87335958	12.04429134

3. Castellana 4x4

Measured exit mass flux and enthalpy values were compared to calculated values from both COBRA-TF and COBRA-EN for channels 5 and 11. In addition, the fluid temperature for these particular channels was evaluated to determine the differences that each code may exhibit between enthalpy and temperature. Two particular runs were chosen to allow for this comparison. Run 60 is a case that utilized a high heat input and a moderate inlet enthalpy to produce boiling conditions in the upper region of the assembly. Run 22 was performed with a low power input and a low inlet enthalpy. This allowed for single phase conditions throughout the assembly and removed the effects on liquid temperature that occur with transition from single-phase to two-phase. Lastly, an additional subcooled boiling case was modeled using all mixing models available in CTF and COBRA-EN. This was done to assess the effects (if any) the mixing model has on the channel mass flux and enthalpy solution. The specific conditions for both runs are shown in Table 3-1. Uncertainty values were not provided for the measured quantities given.

Table 3-1: Test Conditions for Runs 60, 22 and 29 of 4x4

Run #:	60	22	29
Assembly Power (MW):	1.5	0.99	0.99
Pressure (psia):	1200	1200	1200
Hin (btu/lbm):	334	172	420
Gave (Mlbm/hr-ft^2):	0.99	1.01	1.00
Average Hexit (btu/lbm)	550	313	563
Channel 5 Hexit (btu/lbm):	635	355	625
Channel 11 Hexit (btu/lbm):	574	342	623
Channel 5 Gexit (lbm/hr-ft^2):	0.68	0.95	0.74
Channel 11 Gexit (lbm/hr-ft^2):	0.82	1.02	0.88

Before comparing individual channel results, the assembly-averaged enthalpy is analyzed to ensure that both CTF and COBRA-EN are correctly predicting a simple energy balance. The assembly-averaged enthalpy distribution is shown compared to the measured exit value in Figure 3-1.

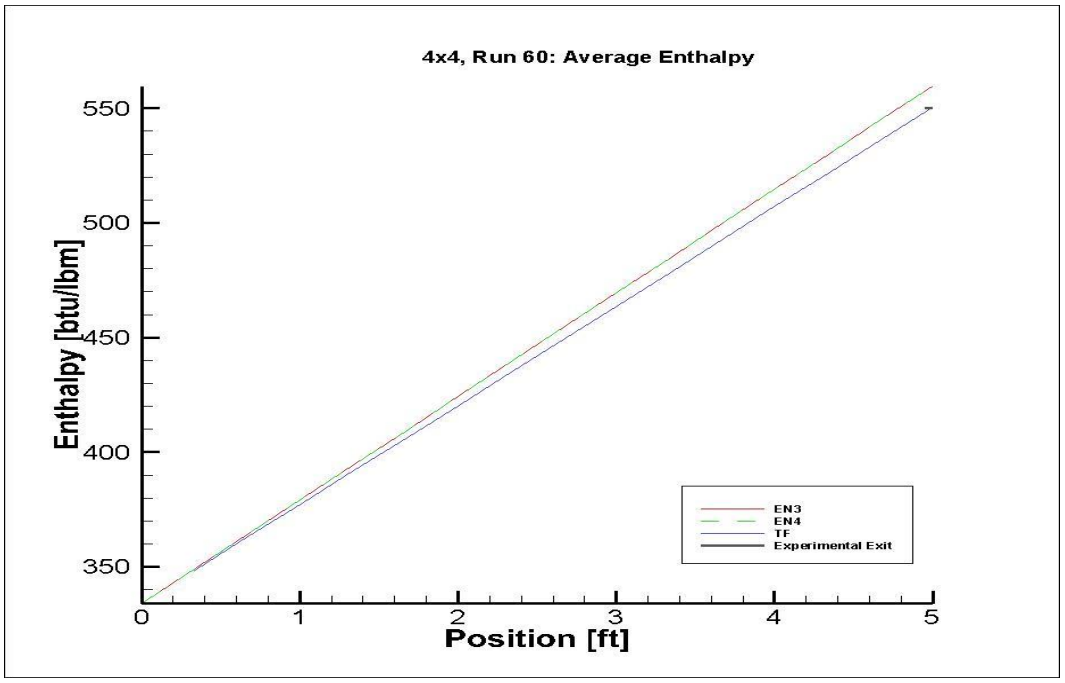

Figure 3-1: Assembly-averaged enthalpy distribution for run 60 of 4x4 bundle

Figure 3-1 shows a linearly increasing enthalpy along the length of the channel, which follows correctly with the axially uniform power profile. Both CTF and the COBRA-EN models predict the exit enthalpy very well. CTF predicts the value almost exactly, while the 3 and 4-equation model in COBRA-EN show a slightly higher exit enthalpy.

The remaining comparisons for Run 60 occur on a specific channel basis. The measured exit mass flux for both channels 5 and 11 are compared to the calculated distribution. These are displayed in Figures 3-2 and 3-3.

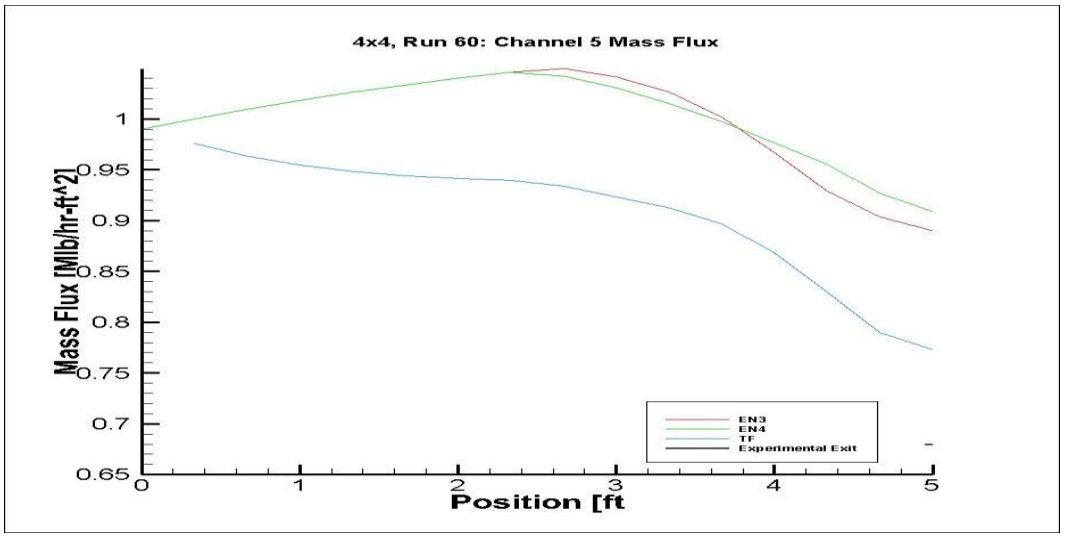

Figure 3-2: Channel 5 mass flux distribution for run 60 of 4x4 bundle

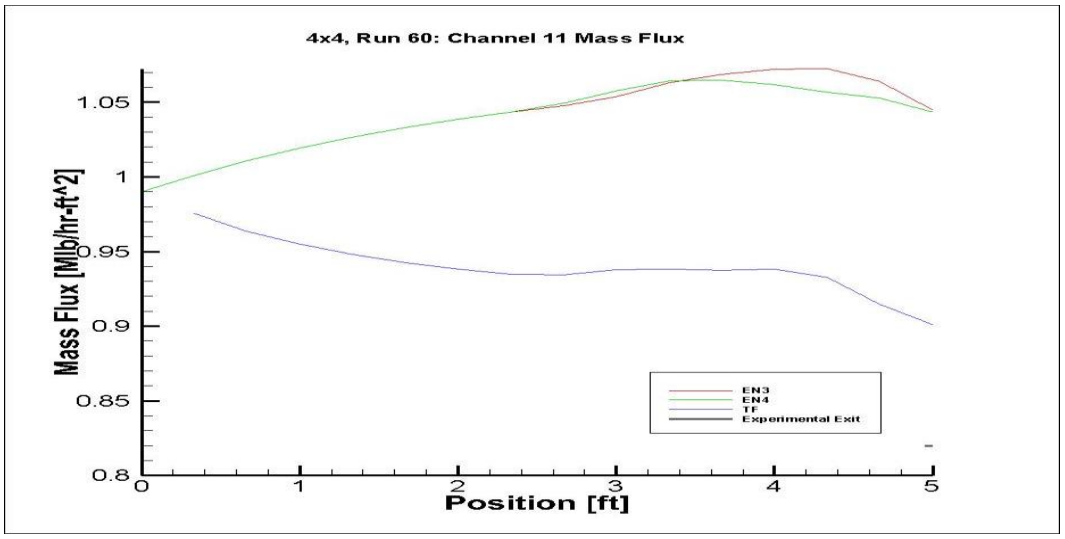

Figure 3-3: Channel 11 mass flux distribution for run 60 of 4x4 Bundle

The calculated distribution for channels 5 and 11 show similar differences between the CTF and COBRA-EN models. The CTF predicted mass flux is of lesser magnitude relative to the COBRA-EN predicted mass flux. In addition, the mass flux decreases over the length of the channel and appears to approach the expected exit value in COBRA-TF.

COBRA-EN produces a behavior that is nearly opposite, showing a channel mass flux that increases slightly over a portion of the channel. For channel 11, this increase occurs over the whole axial length. While neither code accurately predicts the exit mass flux, CTF does appear to be approaching a reasonable solution for both channels.

The measured channel exit enthalpies are shown against the calculated enthalpies in Figures 3-4 and 3-6. In order to understand the relationship between enthalpy and temperature in CTF during subcooled boiling, the liquid phase temperature for each channel is displayed in Figures 3-5 and 3-7.

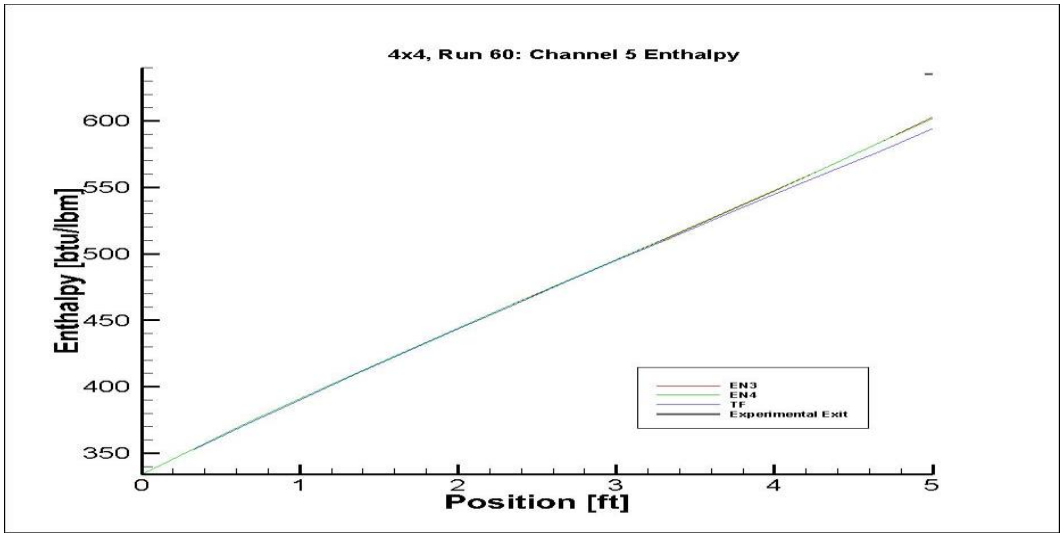

Figure 3-4: Channel 5 enthalpy distribution for run 60 of 4x4 bundle

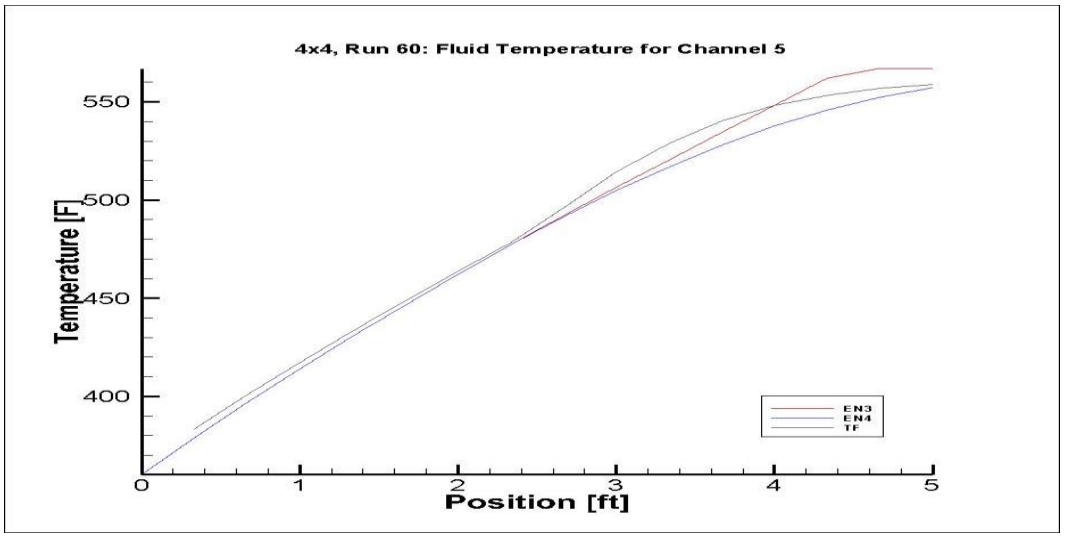

Figure 3-5: Channel 5 liquid phase temperature distribution for run 60 of 4x4 bundle

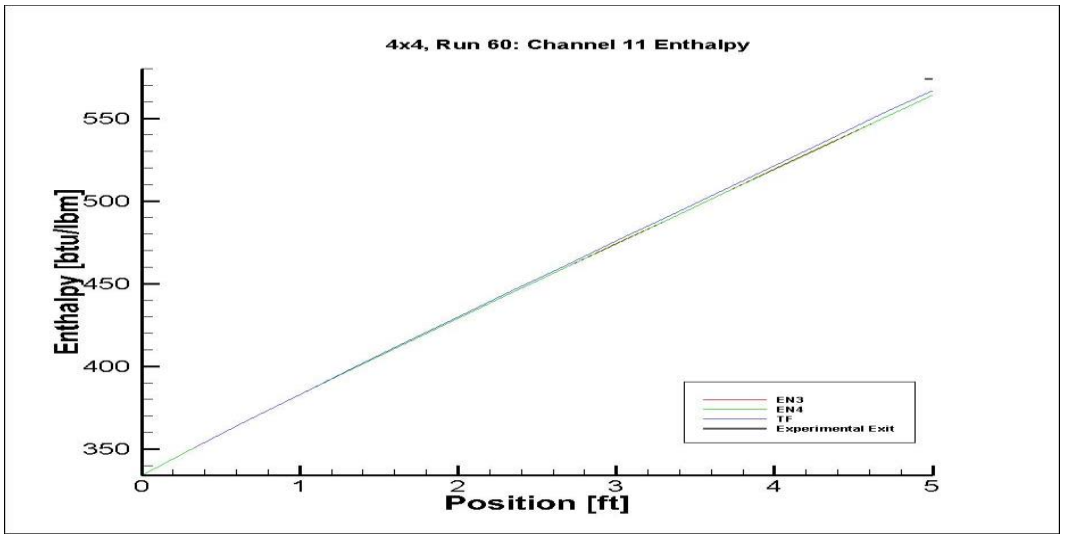

Figure 3-6: Channel 11 enthalpy distribution for run 60 of 4x4 bundle

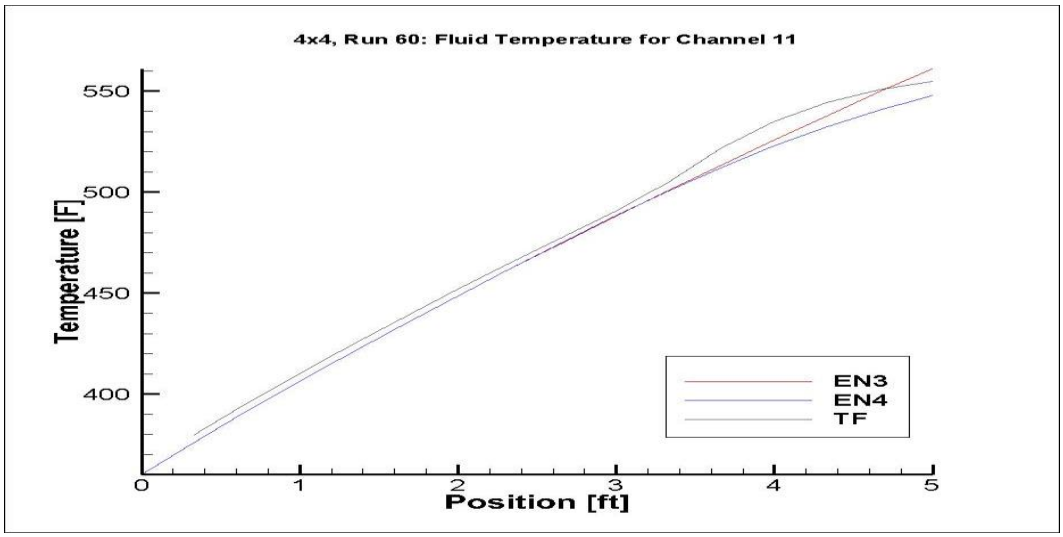

Figure 3-7: Channel 11 liquid phase temperature distribution for run 60 of 4x4 bundle

In Figures-3-4 and 3-6, the channel specific enthalpy is rising correctly according to the uniform axial heat input. The calculated enthalpy for both channels falls below the enthalpies measured at the exit. This behavior is to be expected due to the higher prediction of the mass flux in each channel. The liquid phase temperature profile follows the enthalpy distribution in a near identical manner until the enthalpy approaches the saturation value (571.938 btu/lbm) [9]. At this time, the fluid begins transitioning to two-phase as boiling begins to occur along the heated rods. This leads to the assymptotic behavior in the liquid phase temperature profile as saturation conditions begin to occur. There is an additional effect that is observed in the CTF distribution for both channels. The CTF liquid phase temperature appears to increase more rapidly when boiling begins to occur. This effect is discussed more fully in the following chapter.

Since both CTF and COBRA-EN mispredicted the channel specific mass flux and enthalpy shown for Run 60 (Figures 3-2, 3-3, 3-4 and 3-6), additional comparisons were made for a completely single phase case. This was performed to assess the code's capabilities for pure single-phase conditions and to ensure the two-phase calculations were not a source of error in the mass flux and enthalpy predictions. The channel specific mass flux and enthalpies for Run 22 are displayed in Figures 3-8, 3-9, 3-10 and 3-11. The computed liquid

temperature for this experiment is also shown in Figures 3-12 and 3-13.

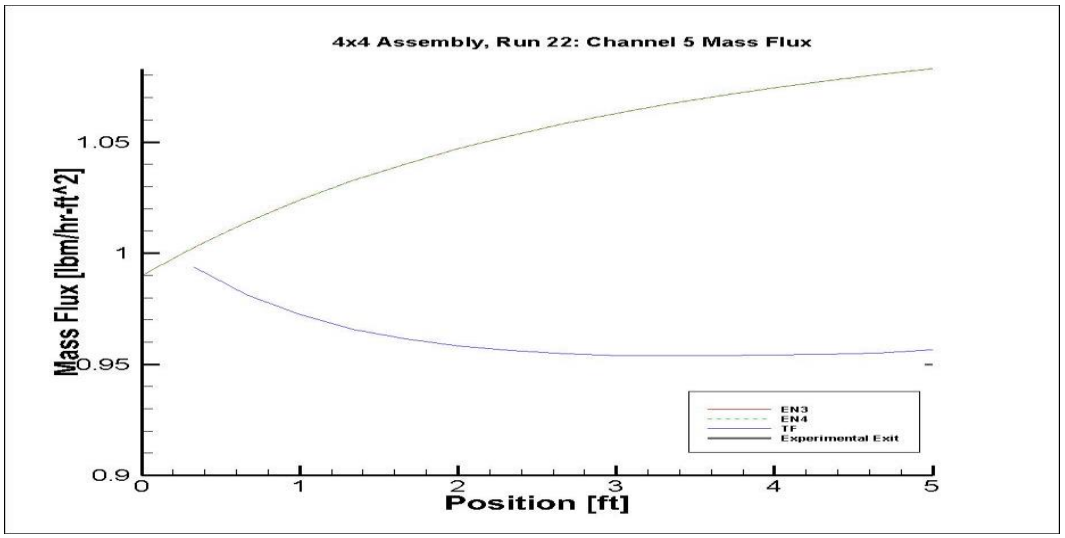

Figure 3-8: Channel 5 mass flux distribution for run 22 of 4x4 bundle

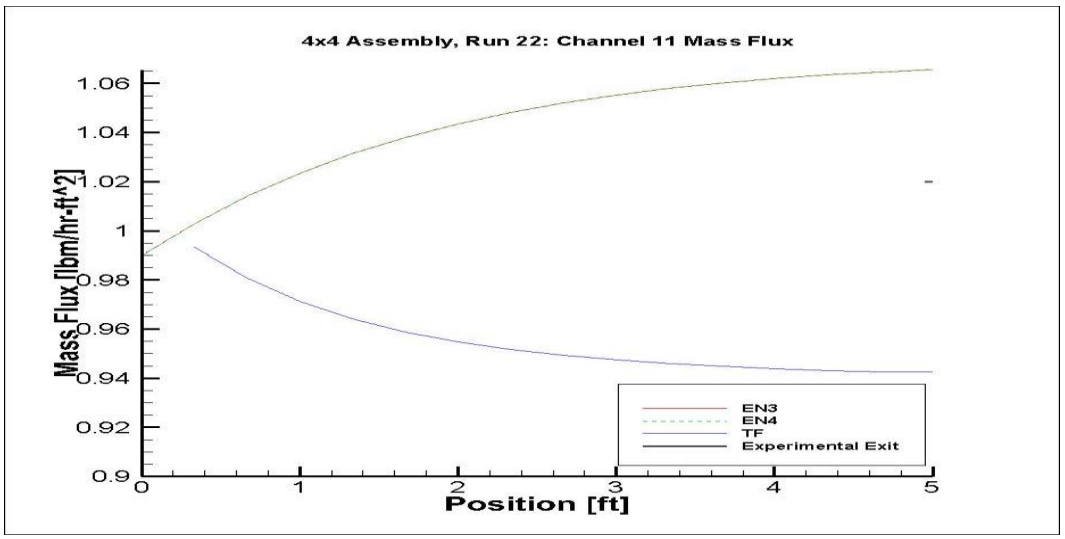

Figure 3-9: Channel 11 mass flux distribution for run 22 of 4x4 bundle

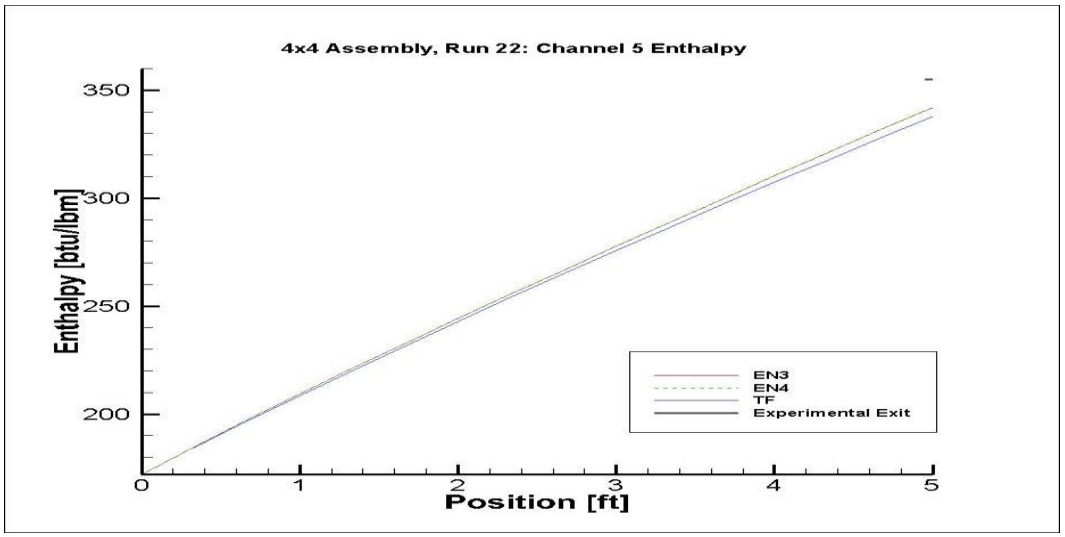

Figure 3-10: Channel 5 enthalpy distribution for run 22 of 4x4 bundle

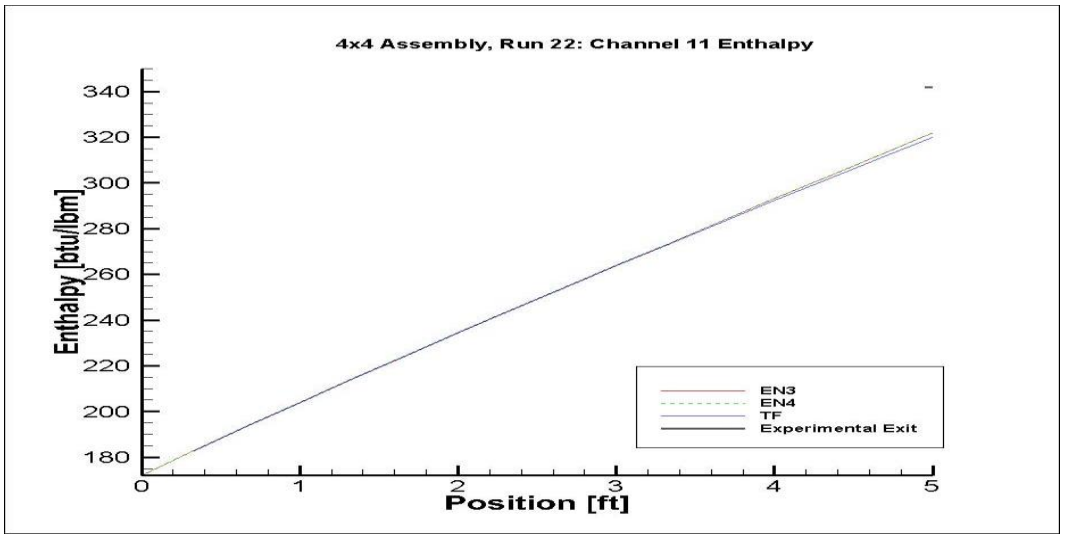

Figure 3-11: Channel 11 enthalpy distribution for run 22 of 4x4 bundle

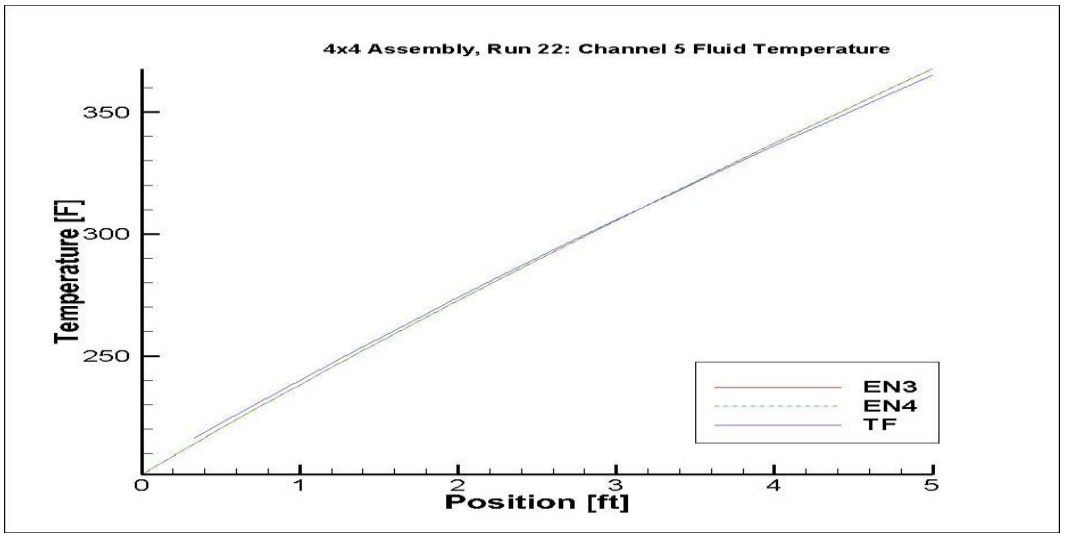

Figure 3-12: Channel 5 liquid phase temperature distribution for run 22 of 4x4 bundle

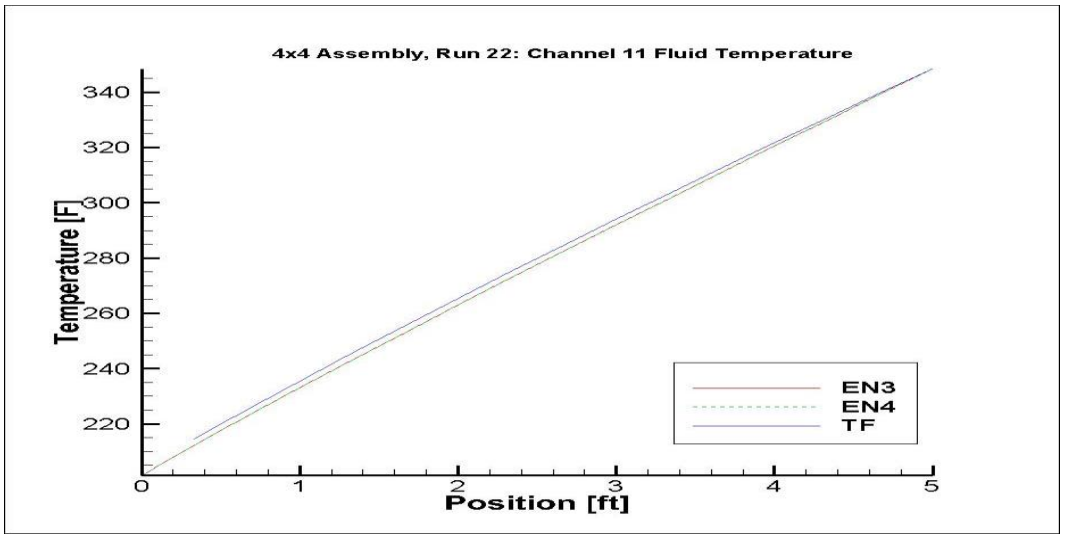

Figure 3-13: Channel 11 liquid phase temperature distribution for run 22 of 4x4 bundle

Figures 3-8 and 3-9 show similar trends in the channel specific mass flux predictions for the single-phase case. Unlike the previous two-phase case, Run 22 displays a smoother distribution of the mass flux along the length of the channel. This is due to the lack of phase transition, and yields a mass flux that shifts only according to geometric considerations (frictional and form losses). For this case, the predicted values behave in a completely opposite manner for CTF and COBRA-EN. CTF predicts a better mass flux for channel 5, but neither code accurately assesses the mass flux for channel 11. For channel 11, the true mass flux is directly in between the calculated values.

In Figures 3-10 and 3-11, it is shown that both codes underpredict the specific enthalpy for each channel, even during single-phase conditions. Unlike the two-phase case, where mass flux was being predicted higher than expected, the values are lower here for CTF. This should yield higher enthalpy predictions, but this does not occur. Additionally, the liquid temperature profiles shown in Figures 3-12 and 3-13 validate the claim that two-phase transition is leading to inaccurate liquid temperature calculations in CTF.

The remaining 4x4 comparisons occurred for run 29. The mass flux and enthalpy for channels 5 and 11 are shown in Figures 3-14, 3-15, 3-16 and 3-17.

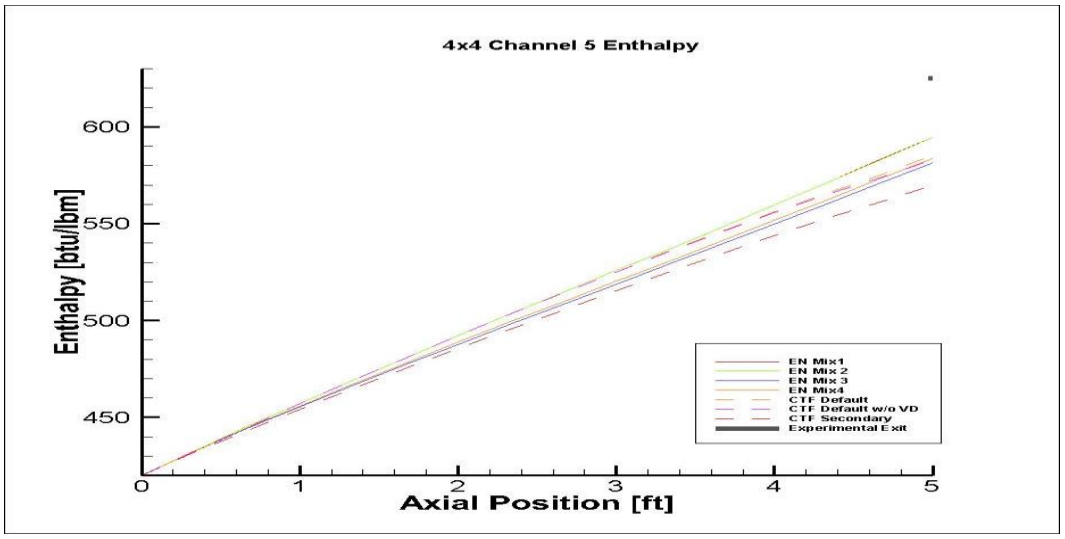

Figure 3-14: Channel 5 enthalpy distribution for run 29 of 4x4 bundle

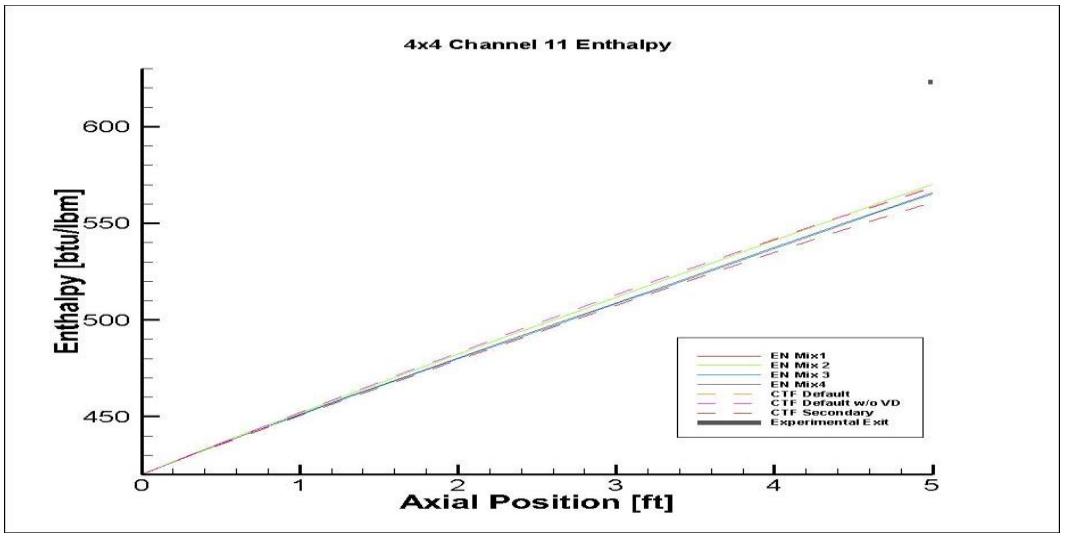

Figure 3-15: Channel 11 enthalpy distribution for run 29 of 4x4 bundle

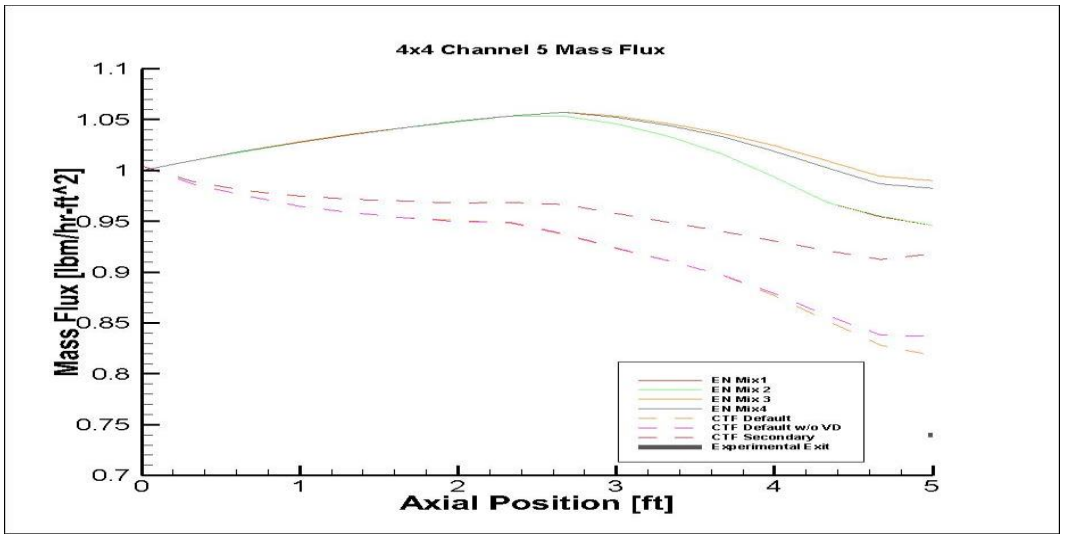

Figure 3-16: Channel 5 mass flux distribution for run 29 of 4x4 bundle

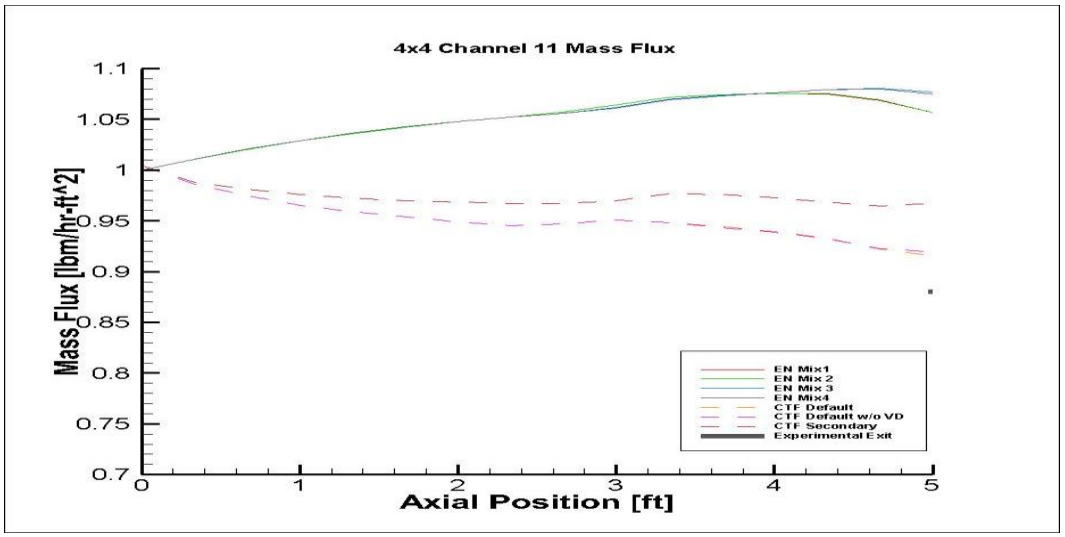

Figure 3-17: Channel 11 mass flux distribution for run 29 of 4x4 bundle

The resulting mass flux and enthalpy shown in Figures 3-14, 3-15, 3-16 and 3-17 were calculated using three mixing models in COBRA-TF and four in COBRA-EN. The mixing models found in COBRA-TF are defined by:

- Default mixing model with void drift taken into account
- Default mixing model without void drift
- Secondary mixing model

The previous 4x4 cases were calculated using the CTF default mixing model with void drift and COBRA-EN model 1. Unlike CTF, COBRA-EN does not account for void drift. The only effect accounted for in COBRA-EN is turbulent mixing, which is modeled by a simple correlation. The turbulent mixing models for both codes and the void drift model in CTF can be found in Appendix A. From the given figures, it is shown that the mixing models does not have a significant effect on the distribution shape. Instead, using a different mixing model shifts the distribution magnitude. For any given mixing model, the calculated exit values do not approach the measured values. This mixing model analysis is applied and discussed further in the 17x17 test case (chapter 5).

4. EPRI 5x5:

The measured quantities for the EPRI 5x5 test assembly include channel exit temperature and the rod surface temperature near the channel exit for the highest powered rod (Rod 25). Comparisons were made based on the calculated rod temperature, the fluid temperature, void fraction and flow quality for the hottest channel (Channel 15). Both of the physical experiments exhibited subcooled boiling in the upper region of the test assembly. Run 55 of Test Assembly 74 was performed at a moderate power input and with a moderate inlet mass flux. This led to single-phase conditions in the majority of the assembly, with subcooled boiling in the upper portion of the assembly. Run 57 of Test Assembly 75 was performed using a high power input and a moderate inlet mass flux. Due to the increased power, a higher degree of subcooled boiling occurred as the fluid closely approaches saturation conditions. Table 4-1 displays the power and inlet conditions for both of these cases. In addition, the measured exit equilibrium quality is given as a measure of the amount of subcooling in each run. The uncertainty values were not provided for the measured quantities.

Table 4-1: Test Conditions for Run 55 and 57 of 5x5 Assemblies

Run #:	55	57
Assembly Power (MW):	2.6472	3.3708
Pressure (psia):	2254	2249
Hin (btu/lbm):	561.5001	563.4802
Gave (lbm/hr-ft^2):	2.6472	2.2306
q''_ave (btu/hr-ft^2)	4.48E+05	5.71E+05
q''_max (btu/hr-ft^2)	5.38E+05	6.88E+05
Exit Equil Qual	-0.080818	-0.005738

The liquid phase temperature and wall temperature comparisons for Channel 15 and Rod 25 of Run 55 are shown in Figures 4-1 and 4-2.

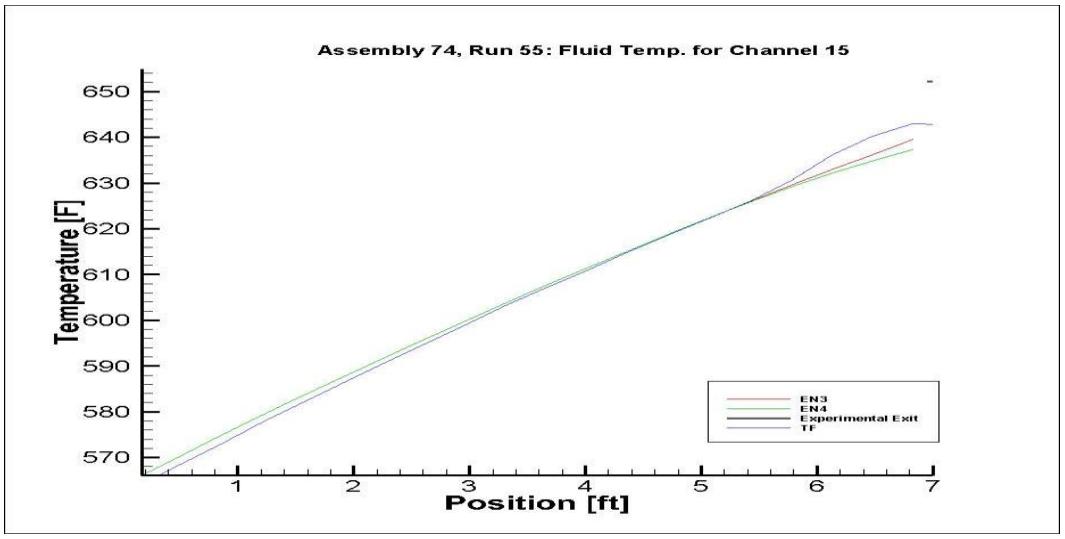

Figure 4-1: Channel 15 liquid phase temperature for run 55 (74) of 5x5 bundle

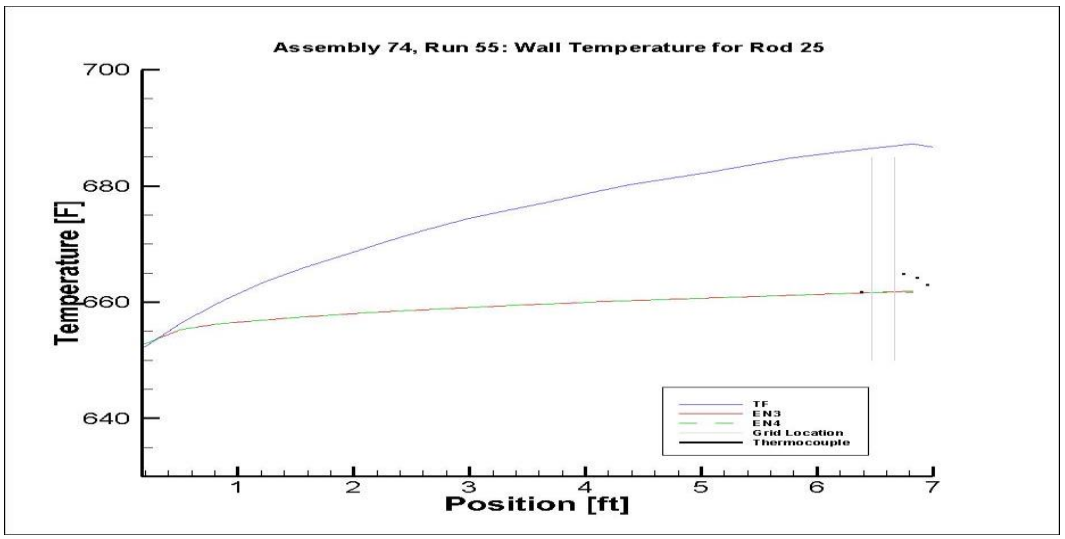

Figure 4-2: Rod 25 wall temperature for run 55 (74) of 5x5 bundle

The calculated liquid temperature for both codes is relatively accurate when compared to the measured exit value. Figure 4-1 displays a temperature distribution that is nearly identical for all three models until approximately 5.5 feet. At this point, the CTF liquid phase temperature increases more rapidly over the remainder of the channel length. Over this same length, the 3 and 4-equation models in COBRA-EN continue to predict a linear increase in the liquid temperature. Differences between the codes is also seen in the wall temperature for Rod 25. Figure 4-2 displays a calculated wall temperature distribution from both models in COBRA-EN that compares reasonably well with the measured values. CTF predicts wall temperatures that are significantly above both the expected values and the COBRA-EN distribution. Neither code appears to capture the effects of the spacer grids on the wall temperature profile. In this region, the measured values show a sharp increase across the length of the spacer grid, while both codes show a smooth transition.

To further understand the effects of two-phase conditions on the calculated wall and liquid phase temperature, the void and flow quality distributions were compared for this case. These values are shown in Figures 4-3 and 4-4. Both figures show similar predicted distributions for both codes. All three models presented show a rapid increase in the void fraction and flow quality in the upper portion of the channel (beyond the bubble departure point). For this case, the 4-equation model in COBRA-EN is predicting the highest magnitude for both void and flow quality following the point of bubble departure. CTF is showing some nominal void fraction occurring prior to this location. When comparing these two plots to the liquid phase temperature distribution (Figure 4-1), it can be noted that the increases in the CTF temperature profile occurs near the location where a non-zero flow quality is found. The effect of two-phase calculations on this temperature profile is analyzed in section 6.2.

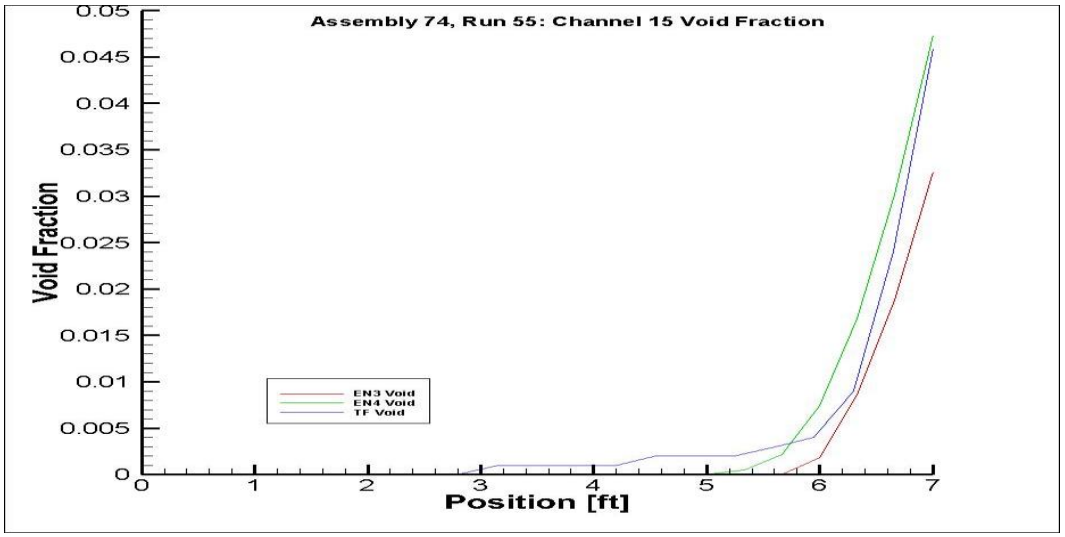

Figure 4-3: Channel 15 void distribution for run 55 (74) of 5x5 bundle

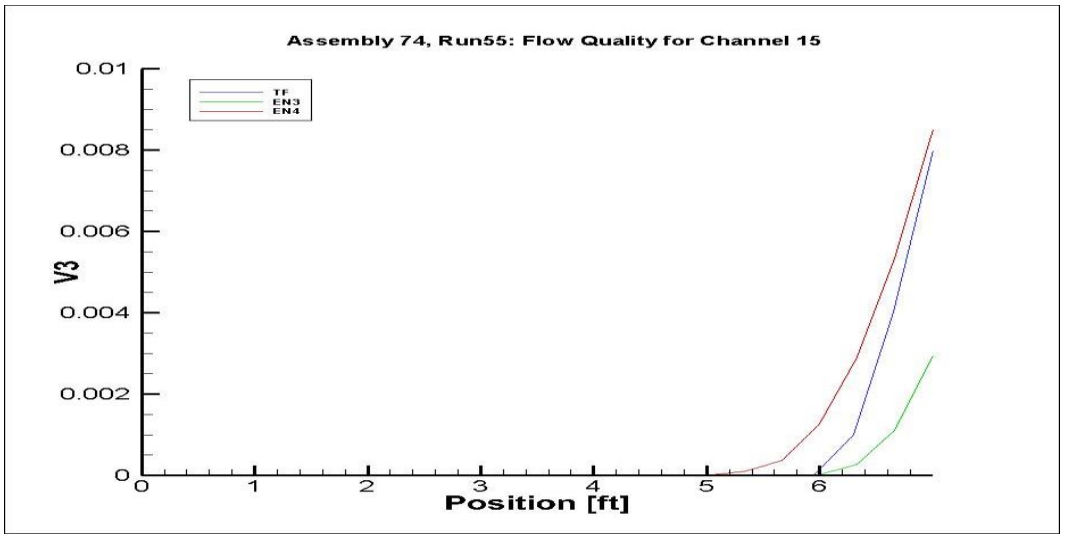

Figure 4-4: Channel 15 flow quality distribution for run 55 (74) of 5x5 bundle

The second 5x5 experiment had a higher heat input and slightly lower inlet mass flow rate. In addition, the pitch and rod-to-wall spacing varied from Assembly 74 to 75. With the higher heat input, more subcooled boiling occuring within the assembly. The effect that this has on the liquid phase temperature in the hottest channel can be viewed in Figure 4-5. In

addition, the wall temperature profile for the highest powered rod is shown in Figure 4-6. For this case, the 4-equation model's results were not obtained as it failed to converge under these conditions.

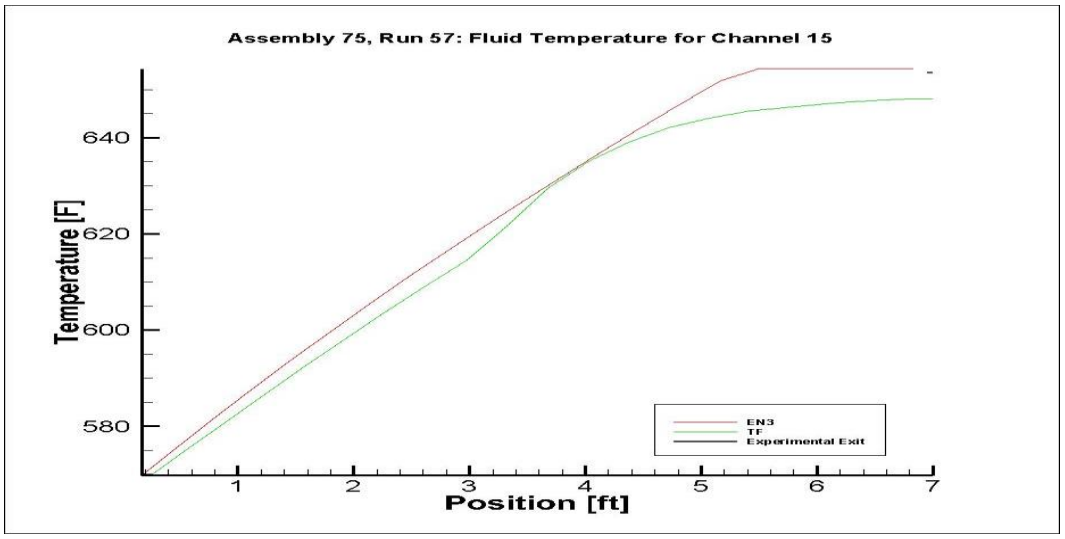

Figure 4-5: Channel 15 liquid phase temperature for run 57 (75) of 5x5 bundle

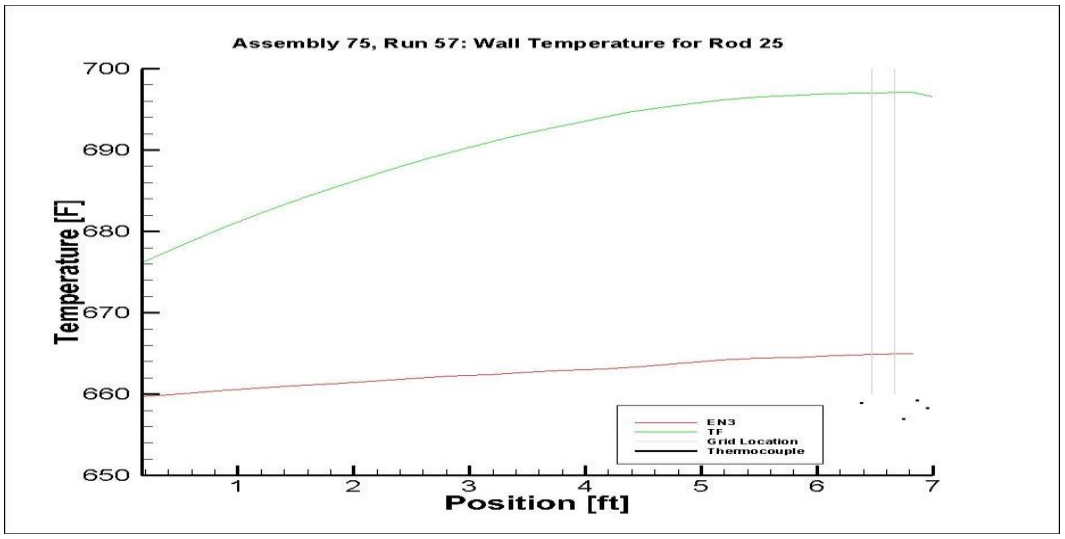

Figure 4-6: Rod 25 wall temperature for run 57 (75) of 5x5 bundle

The temperature in Figure 4-5 adequately represents the fluid nearing saturation conditions. Both codes show the temperature approach an asymptotic value that is associated with the saturation temperature. COBRA-TF is predicting an exit temperature that is a few degrees lower than the measured value, while COBRA-EN is calculating a reasonable exit value. Similarly to Run 55 of Assembly 74, the liquid phase temperature in CTF departs from a linear increase earlier than expected. However, following this effect the temperature profile does behave as expected for a fluid approaching saturation. The CTF wall temperature shown is behaving as the previous case with significantly higher calculated values relative to the measured and COBRA-EN values. Unlike the previous case, the over prediction in the wall temperature begins at the bottom of the rod.

Further assessing this case required the void fraction and flow quality for channel 15. These distributions are shown in Figures 4-7 and 4-8.

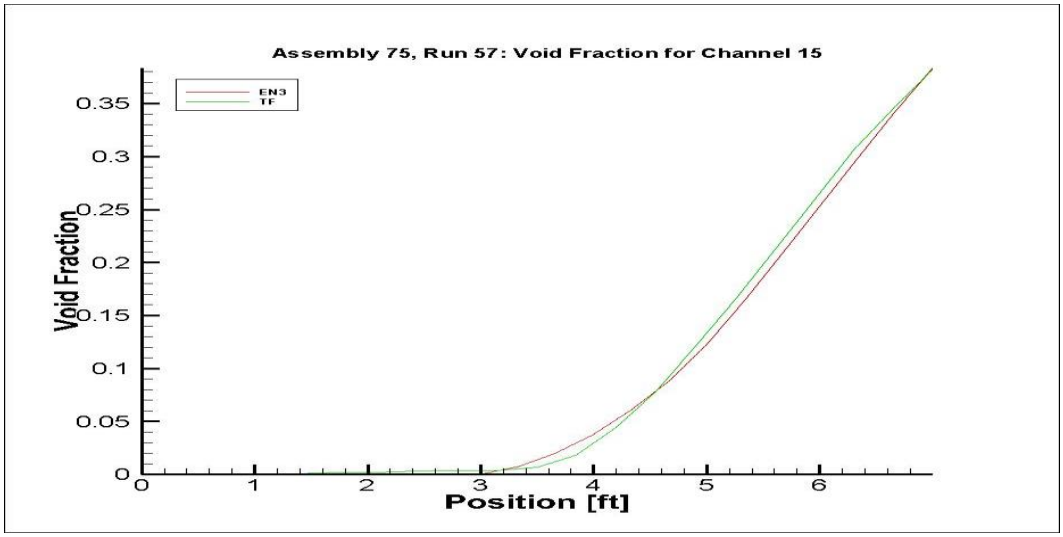

Figure 4-7: Channel 15 void fraction for run 57 (75) of 5x5 bundle

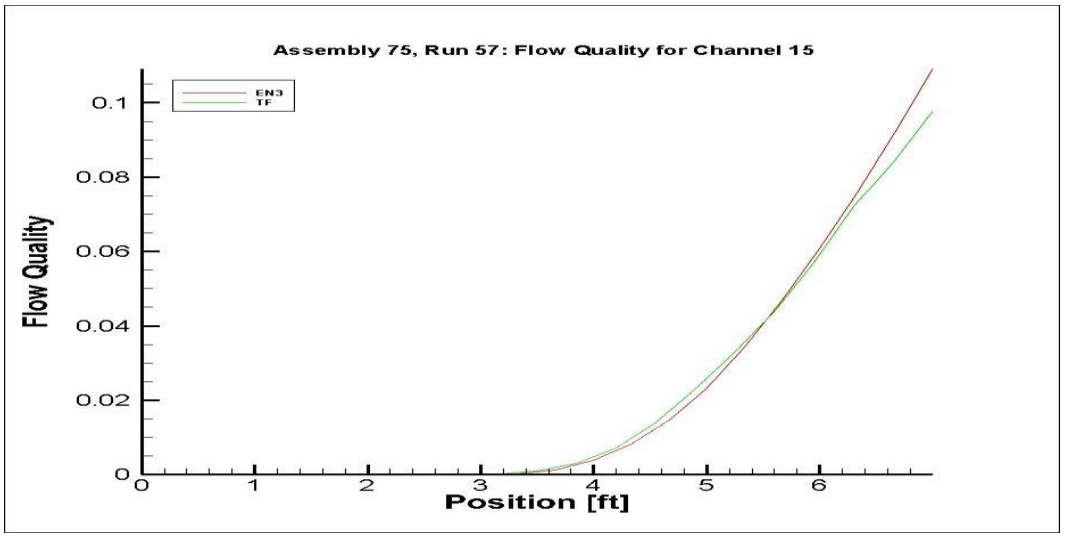

Figure 4-8: Channel 15 flow quality for run 57 (75) of 5x5 bundle

The void fraction and flow quality behave almost identically to the previous cases examined, with the main exception being the location at where they begin to develop in the channel. Each distribution is zero for a portion of the channel, before the point of bubble departure. They then rapidly increase over the remaining length of the channel. Both the 3-equation model in COBRA-EN and the CTF model display similar distributions/magnitudes for void and flow quality. The method of flow quality and bubble departure calculation for each code is found in section 6.1.

5. Standard 17x17 Assembly

A standard Westinghouse 17x17 assembly was used to evaluate the turbulent mixing calculations in COBRA-TF. For the normal operating conditions, the average fluid exit temperature will be subcooled. The hot subchannel will contain as much as 30% void at the exit [5]. The mixing model in CTF was compared to the four mixing models found in COBRA-EN for the highest powered channel. In addition, the various spatial heat conduction options available in CTF were used to ascertain any effects that may occur by modeling heat conduction in the axial and azimuthal directions. The default heat conduction model in CTF assumes conduction in the radial direction only. Radial heat conduction is the only available option in COBRA-EN. The test conditions were previously outlined in Table 2-6. The total heat input for the highest powered assembly is 22.757 megawatts.

The wall temperature profile for a heated rod adjacent to four other heated rods is shown in Figure 5-1. In addition, the wall temperature for a heated rod adjacent to a water rod is shown in Figure 5-2. While COBRA-TF does have the ability to modify the heat generation in the radial direction for each rod, these tests occurred with a radially uniform volumetric heat generation profile.

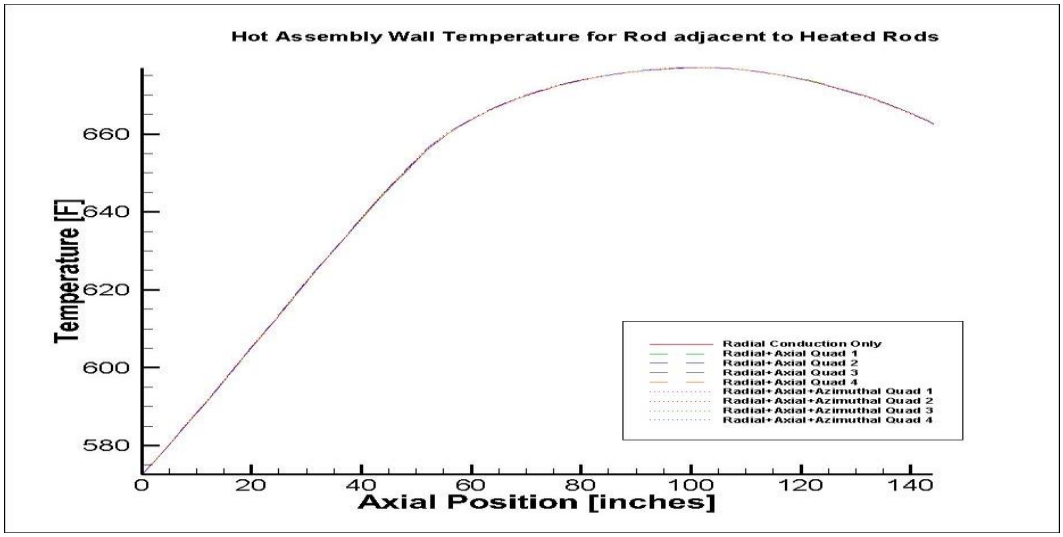

Figure 5-1: Heat conduction comparisons for a heated rod adjacent to heated rods in 17x17 assembly

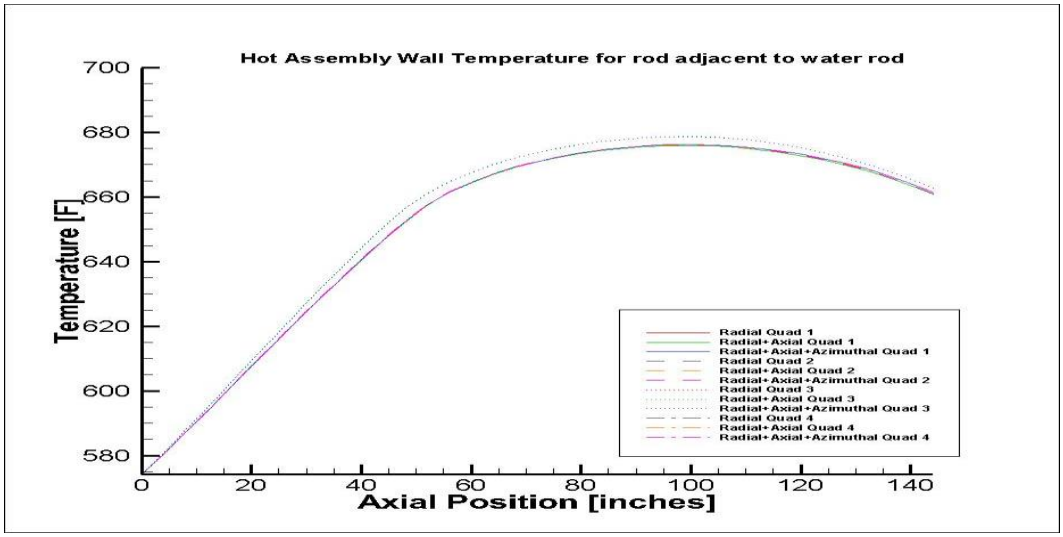

Figure 5-2: Heat conduction comparisons for a heated rod adjacent to water rod in 17x17 assembly

The wall temperature profiles presented are for:

- Radial conduction only
- Radial and axial conduction in the four azimuthal quadrants
- Radial, axial and azimuthal conduction in the four azimuthal quadrants

From Figure 5-1, it is shown that there are no significant variations in the wall temperature profile due to increased conduction dimensionality. In addition, for the higher dimensionality models, no differences can be observed in any of the four quadrants. This is not the case for the wall temperature shown in Figure 5-2. There is some variation in the wall temperature in each quadrant, with the most noticeable occurring in the third quadrant. However variation is not necessarily due to the increased conduction dimensionality. Instead it could occur from the reduced fluid temperature in the subchannel near the water rod, which would drive the rod surface heat transfer in that quadrant.

The mixing models available in COBRA-TF were compared to those used in COBRA-EN for the hottest channel in the 17x17 assembly. The calculated enthalpy and mass flux within the channel for each respective mixing model is shown in Figures 5-2 and 5-3.

There were two mixing models available in COBRA-TF, and each model could be implemented with or without the effects of void drift.

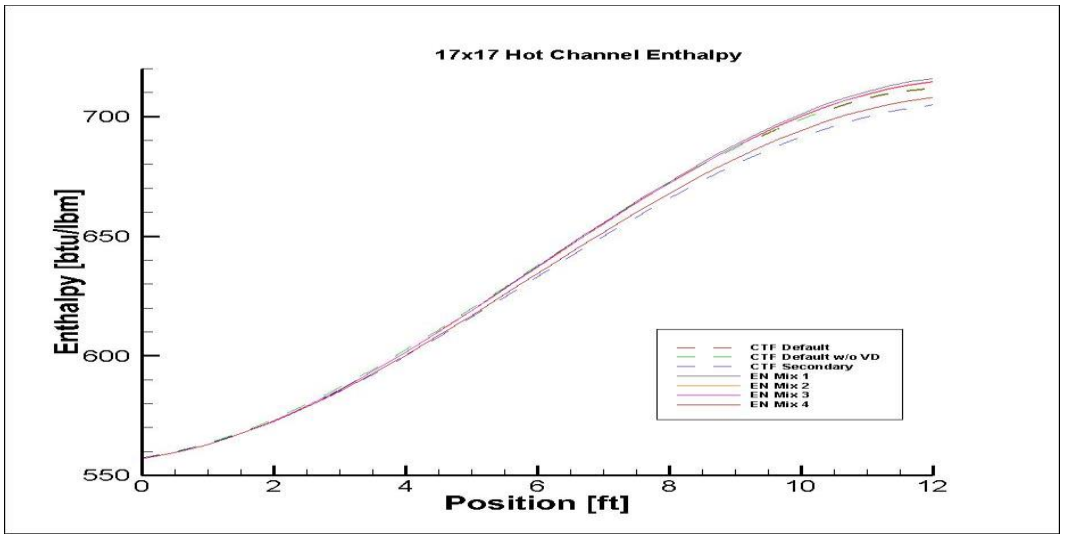

Figure 5-3: Enthalpy for mixing model comparisons in hot channel of 17x17 assembly

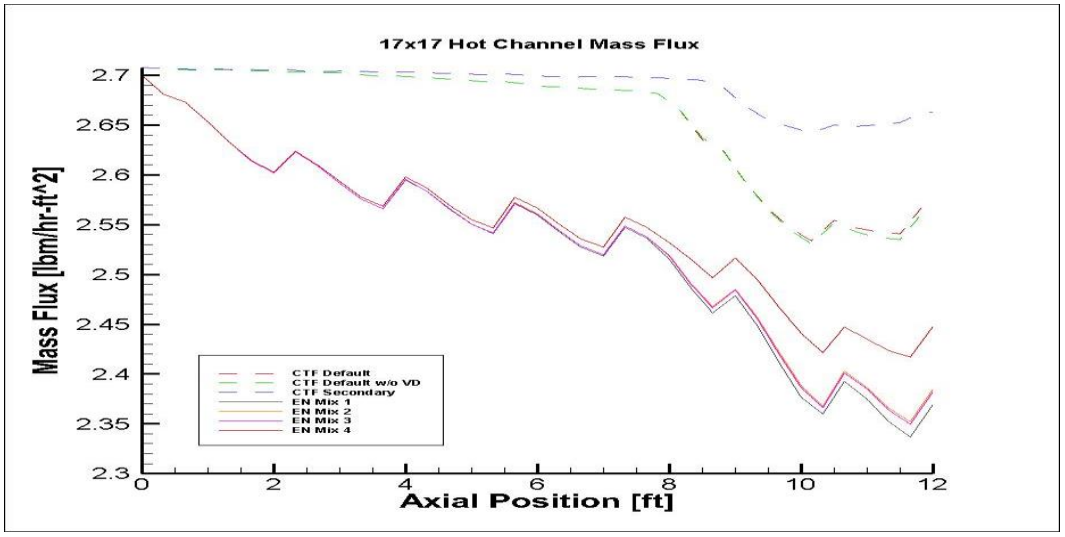

Figure 5-4: Mass flux for mixing model comparisons in hot channel of 17x17 assembly

The enthalpy profiles shown in Figure 5-2 are typical of those for a cosine shaped power profile. There are slight variations that occur in the enthalpy values depending on the mixing model, but these differences are not significant in magnitude and do not alter the shape of the profile. Unlike the enthalpy, the mass flux in the channel varies significantly depending on the model chosen. Both COBRA-TF and COBRA-EN are showing a decreasing mass flux with increasing axial position. The models found in COBRA-EN are displaying lower values for the mass flux along the whole length of the channel. In addition, the location of spacer grids are noted for COBRA-EN as the mass flux distribution displays small sharp increases near spacer grid locations. The CTF distributions are relatively linear until about 8 feet into the channel. At this point, there is a rapid decrease in the mass flux for the three CTF mixing models. The only noticeable effect in the CTF prediction due to spacer grids occurs near the channel exit. Reasons for the higher mass flux found in CTF is discussed in section 6.3.

6. Discussion and Physical Model Comparisons

6.1 Void Appearance and Flow Quality

At the onset of the simulation, CTF assumes the presence of all phases. There is no code logic that accounts for phase appearance or disappearance. In order for the solution procedure to proceed smoothly, CTF imposes a small non-zero value as a minimum for the vapor void fraction whether the fluid should be all single-phase liquid or not. This allows the fluid be approximated as single-phase prior to boiling conditions. The vapor void fraction minimum used in CTF is 10^{-6}. This method requires the solution of all phasic equations from the beginning of the simulation and is also used in RELAP-5 [7]. In RELAP, the void minimum value is set to 10^{-5}.

CTF has no bubble departure criteria. The calculation of flow quality is simply evaluated from the phasic mass fluxes. The flow quality is defined as:

$$x = \frac{G_v}{G_v + G_l} \tag{6.1}$$

where the phasic mass flux is given as a magnitude quantity. This quantity is calculated by accounting for both axial and lateral mass flux contributions.

$$G_k = \sqrt{G_{z,k}^2 + G_{y,k}^2} \tag{6.2}$$

$G_{z,k}$ is the axial mass flux due to phase k at the current cell. $G_{y,k}$ is the average lateral mass flux from the surrounding subchannels due to phase k. Each mass flux constituent (axial or lateral) is defined by:

$$G_{i,k} = \alpha_{i,k}\rho_{i,k}v_{i,k} \tag{6.3}$$

Even though void is always assumed to exist within the channel, flow quality does not begin

to develop until a vapor velocity that is greater than zero (either axial or lateral) is obtained.

This is a completely different method from the ones utilized in COBRA-EN. The 3-equation model found in COBRA-EN allows the user to pick one of two empirical correlations for evaluating flow quality. The two models available are defined as follows:

1. EPRI Correlation (default)

$$x = \frac{x_e - x_d\left(1 - \tanh\left(1 - \frac{x_e}{x_d}\right)\right)}{1 - x_d\left(1 - \tanh\left(1 - \frac{x_e}{x_d}\right)\right)} \tag{6.4}$$

Where,

$$x_e = \frac{h - h_f}{h_{fg}} \tag{6.5}$$

$$x_d = -\frac{c_{pl}Z}{h_{fg}} \tag{6.6}$$

$$Z = \frac{B - \sqrt{B^2 - 4AC}}{2A} \tag{6.7}$$

$$A = 4C_b(h_{db} + h_{HN})^2 \tag{6.8}$$

$$B = 2h_{db}^2(h_{HN} + 0.5h_{db}) + 8q''C_b(h_{HN} + h_{db}) \tag{6.9}$$

$$C = 4C_b q''^2 + q'' h_{db}^2 \tag{6.10}$$

$$h_{db} = 0.023 Re_l^{0.8} Pr_l^{0.4}\left(\frac{k_l}{D_e}\right) \tag{6.11}$$

$$h_{HN} = 0.2 Re_l^{0.662} Pr_l\left(\frac{k_l}{D_e}\right) \tag{6.12}$$

$$C_b = 0.05358 e^{\frac{P}{630}} \tag{6.13}$$

2. Levy Model

$$x = x_e - x_d e^{\frac{x_e}{x_d}-1} \tag{6.14}$$

$$x_d = -\frac{c_{pf}\Delta T_d}{h_{fg}} \tag{6.15}$$

Where,

$$\Delta T_d = \frac{q^{'}}{P_h h_f} \quad if \;\; Y_B^+ < 0 \tag{6.16}$$

$$\Delta \mathrm{T_d} = \frac{q^{'}}{P_h h_f} - (Q)(\mathrm{Pr})(\mathrm{Y_B^+}) \;\; 0 \le \mathrm{Y_B^+} \le 5 \tag{6.17}$$

$$\Delta \mathrm{T_d} = \frac{\mathrm{q^{'}}}{\mathrm{P_h h_f}} - 5Q\left[Pr + \ln\left(1 + Pr\left(\frac{Y_B^+}{5} - 1\right)\right)\right] \;\; 5 < Y_B^+ < 30 \tag{6.18}$$

$$\Delta \mathrm{T_d} = \frac{\mathrm{q^{'}}}{\mathrm{P_h h_f}} - 5Q\left[Pr + \ln(1 + 5\mathrm{Pr}) + 0.5\ln\left(\frac{Y_B^+}{30}\right)\right] \;\; Y_B^+ \ge 30 \tag{6.19}$$

And,

$$Y_B^+ = \frac{0.015}{\mu_f}\left(\frac{\sigma g_c D_h}{\nu_f}\right)^{0.5} \tag{6.20}$$

$$Q = \frac{\frac{q^{'}}{Ph}}{c_{pf}\left(\rho_f \tau_w g_c\right)^{0.5}} \tag{6.21}$$

$$\tau_w = \frac{0.125 f \nu_f G^2}{g_c} \tag{6.22}$$

With the bubble departure quality (x_d) known, the flow quality can be obtained

In addition, an iterative method is used to calculate flow quality if the user chooses the 4-equation model found in COBRA-EN. The iteration process occurs as:

Given a previous α, slip ratio and slip difference (dS) value, the flow quality is calculated directly:

$$x^p = \frac{\alpha_g^p \rho_v}{\alpha_g^p \rho_v + \frac{\left(1-\alpha_g^p\right)\rho_l}{S^p}}$$

$$if(x^p \leq 0 \; or \; x^p \geq 1) \quad \alpha_g = 0$$

$$if\left(\alpha_g^p > 0 \; and \; \alpha_g^p < 1\right)$$

$$S = S + dS^p * d\alpha_g$$

$$\alpha_g^{p+1} = \alpha_g^p + d\alpha_g$$

$$x^{p+1} = \frac{\alpha_g^{p+1}\rho_v}{\alpha_g^{p+1}\rho_v + \frac{\left(1-\alpha_g^{p+1}\right)\rho_l}{S^{p+1}}}$$

Where,

$d\alpha_g = 0.001$

At some point over the length of a boiling channel, the flow quality will become a positive quantity. This iterative method assumes a previous void fraction value is known beforehand. The location where a non-zero void fraction is calculated in the 4-equation model is determined through a vapor generation correlation. The model is shown in Equation 6.23.

$$\Gamma_v''' = \left[\frac{P_h \Delta z}{h_{fg}(1+\beta)}\right]\left[\frac{q'' H_m}{H_{thom}+H_{db}} - \left(\frac{H_{db}H_m}{H_{thom}+H_{db}} + H_{hn}\right)(T_{sat}-T_l)\right] \tag{6.23}$$

$$\beta = \max\left[0.0, \left(\frac{h_f - h_l}{h_g - h_l}\right)\left(\frac{\rho_l}{\rho_g}\right)\right] \tag{6.24}$$

$$H_{thom} = 0.05358 e^{\frac{P}{630}}(T_w - T_{sat}) \tag{6.25}$$

$$H_m = H_{thom} + \frac{1}{2}H_{db} \tag{6.26}$$

$$H_{db} = 0.023 Re_l^{0.8} Pr_l^{0.4} \left(\frac{k_l}{D_h}\right) \quad (6.27)$$

$$H_{hn} = 0.2 Re_l^{0.662} Pr_l \left(\frac{k_l}{D_h}\right) \quad (6.28)$$

When the wall temperature exceeds the saturation temperature, the vapor generation term is activated. This will lead to a non-zero source term in the vapor conservation equation, which results in the calculation of a non-zero void fraction and flow quality from the previously outlined iteration process.

6.2 Liquid and Wall Temperature under subcooled boiling conditions

When flow quality begins to develop, there is a noticeable increase in the liquid phase temperature calculated in CTF. This effect was captured in Figure 4-1. For subcooled regions, the liquid phase temperature is dependent only on the liquid enthalpy. This leads to the conclusion that CTF is over predicting the liquid enthalpy, while preserving the correct total enthalpy. This is due to an incorrect partitioning of heat input to the fluid. For normal flow regimes (defined in CTF as Tw<Tchf *), the wall heat flux is allocated only to the liquid phase. While this assumption is accurate for an annular flow regime, it is not valid for subcooled boiling conditions. The wall heat flux will only be partitioned to the vapor phase when the vapor volume fraction exceeds 0.999. At this point, the vapor phase will receive the total wall heat flux. Under hot wall flow regimes (Tw>Tchf), there is more of a partitioning (weighting) effect that occurs with the wall heat flux.

In CTF, the total wall heat transfer is evaluated according to the Chen correlation. The total heat transfer coefficient for subcooled and saturated nucleate boiling is given by:

$$h_{chen} = h_{fc} + h_{nb} \quad (6.29)$$

Where h_{fc} is a modified Dittus-Boelter correlation:

$$h_{fc} = 0.023 F_{chen} \left(\frac{k_l}{D_h}\right) Re_l^{0.8} \mathrm{Pr}^{0.4} \tag{6.30}$$

$$F_{chen} = \begin{matrix} 1.0 & if\ \chi_{TT}^{-1} < 0.1 \\ 2.34(\chi_{TT}^{-1} + 0.213)^{0.736} & if\ \chi_{TT}^{-1} > 0.1 \end{matrix} \tag{6.31}$$

*Note: Tchf in CTF is given by: $Tchf = (T_{sat} + 75)°\mathrm{F}$

$$\chi_{TT}^{-1} = \left(\frac{x}{1-x}\right)^{0.9} \left(\frac{\rho_f}{\rho_g}\right)^{0.5} \left(\frac{\mu_g}{\mu_f}\right)^{0.1} \tag{6.32}$$

F_{chen} will be 1.0 in the case of subcooled boiling. The nucleate boiling coefficient is given by:

$$h_{nb} = 0.00122 S_{chen} \left(\frac{k_f^{0.79} Cp_f^{0.45} \rho_f^{0.49} g_c^{0.25}}{\sigma^{0.5} \mu_f^{0.29} h_{fg}^{0.24} \rho_g^{0.24}}\right) (T_w - T_{sat})^{0.24} \left(P(T_w) - P(T_{sat})\right)^{0.75} \tag{6.33}$$

Where,

$$S_{chen} = \begin{matrix} \left(1 + 0.12 Re_{2\phi}^{1.14}\right)^{-1} & if\ Re_{2\phi} < 32.5 \\ \left(1 + 0.42 Re_{2\phi}^{0.78}\right)^{-1} & if\ 32.5 < Re_{2\phi} < 50.9 \\ 0.1 & Re_{2\phi} > 50.9 \end{matrix} \tag{6.34}$$

$$Re_{2\phi} = (10^{-4}) Re_l F_{chen}^{1.25} \tag{6.35}$$

$$P(T_w) - P(T_{sat}) = \left[\frac{5.4042 h_{fg}}{\nu_{fg}(T_{sat} + 460)}\right] (T_w - T_{sat})^A \tag{6.36}$$

$$A = \frac{1.0306}{(\log_{10} P)^{0.017}} + \frac{0.0020632}{(\log_{10} P)^{1.087}} \max\{0.0, (T_w - T_{sat}) - 5.0\} \quad (6.37)$$

In COBRA-EN, the user has the option to pick the heat transfer correlation to be used for boiling conditions. The following models are available for subcooled and saturated nucleate boiling:

1. Thom Correlation:

$$T_w = 0.072(3600q'')^{0.5} e^{-\frac{P}{1260}} \quad (6.38)$$

$$\Delta T_w = T_w + T_{sat} - T_\infty \quad (6.39)$$

$$h_{thom} = \frac{q''}{\Delta T_w} \quad (6.40)$$

2. Thom + single-phase:

$$h_{sp} = 3600 * h_{fc} \quad (6.41)$$

$$A = \left(\frac{1}{0.072 e^{-\frac{P}{1260}}} \right)^2 \quad (6.42)$$

$$\Delta = \left(h_{sp}\right)^2 + 4A \left(3600q'' - h_{sp}(T_{sat} - T_\infty)\right) \quad (6.43)$$

$$T_w = T_{sat} - \frac{h_{sp} - \sqrt{\Delta}}{2A} \tag{6.44}$$

$$\Delta T_w = T_w - T_\infty \tag{6.45}$$

$$h = \frac{q''}{\Delta T_w} \tag{6.46}$$

3. Jens-Lottes:

$$T_w = 1.9(3600q'')^{0.25} e^{-\frac{P}{900}} \tag{6.47}$$

$$\Delta T_w = T_w + T_{sat} - T_\infty \tag{6.48}$$

$$h = \frac{q''}{\Delta T_w} \tag{6.49}$$

4. Rohsenow:

$$a_1 = \sqrt{\left(\frac{\sigma}{\rho_l - \rho_g}\right)} \tag{6.50}$$

$$a_2 = \frac{1}{\mu h_{fg}} \tag{6.51}$$

$$a_3 = \frac{\mu h_{fg}}{k} \tag{6.52}$$

$$T_w = 0.0132(q'' a_1 a_2)^{\frac{a_3}{3}} \tag{6.53}$$

$$\Delta T_w = T_w + T_{sat} - T_\infty \tag{6.54}$$

$$h = \frac{q''}{\Delta T_w} \tag{6.55}$$

It should also be noted that the Chen correlation utilized in COBRA-TF is not valid for rod bundles under highly subcooled boiling and high pressure conditions. This correlation was developed to evaluate wall heat transfer in round tubes under saturated boiling conditions and forced convection vaporization in low pressure systems [8]. For the subcooled boiling conditions used in the test cases, this heat transfer correlation is shown to severely over predict the wall temperature. This heat transfer correlation is used in CTF for any given normal wall (non-CHF) flow condition. The use of this correlation for such a wide range of flow regimes would lead to inaccurate results for numerous reactor flow simulations. The default heat transfer correlation (Thom+single-phase) used in COBRA-EN was found to produce reasonably accurate results. As a result of this study, the Thom correlation has since been added as an option in COBRA-TF.

RELAP-5 allows the wall heat flux calculation to come directly from a correlation package based on the current flow regime. This package computes the heat flux to each phase directly, with no need for an additional partitioning scheme. If the correlation package is not used, and the total heat flux is computed from an appropriate correlation, a partitioning scheme is used. The total heat flux is distributed to each phase in direct proportion with that phase's volume fraction.

Additional heat source concerns which would cause this effect may result from the way interfacial heat transfer is handled in CTF. The interfacial heat transfer to the liquid is evaluated with the following correlations:

Superheated Liquid:

$$h_{shl,i} = \max\left(h_{conv,i}, h_{cond,i}\right) A_i + h_{nb} A_{pw} \tag{6.56}$$

Where,

$$h_{conv,i} = \frac{k_f}{D_b}\left(2.0 + 0.74 Re_b^{0.5} \mathrm{Pr}^{\frac{1}{3}}\right) \tag{6.57}$$

$$h_{cond,i} = \frac{k_f}{D_b} Ja \tag{6.58}$$

$$Ja = \frac{\rho_l\left(h_l - h_f\right)}{\rho_v h_{fg}} \tag{6.59}$$

$$h_{nb} = \frac{k_f}{D_b} \max\left(8.0, 0.023\left(\frac{\rho_l v_l D_b}{\mu_m}\right)^{0.8} Pr^{0.4}\right) \tag{6.60}$$

$$\mu_m = \mu_l (1 - \alpha_v)^{-\frac{2.5(\mu_v + 0.4\mu_l)}{\mu_v + \mu_l}} \tag{6.61}$$

$$D_b = 2 r_b \tag{6.62}$$

Subcooled Liquid:

$$h_{scl,i} = 1.1284 \sqrt{\frac{k_f}{D_b} v_l \rho_l c_{p,l}} A_i \tag{6.63}$$

The interfacial vapor heat transfer is dealt with in a completely different manner. It is defined as:

$$h_{v,i} = \left(2.78 \frac{btu}{s - ft^2 - F}\right) A_i \tag{6.64}$$

This model is used for both a subcooled or superheated vapor. This would yield a heat source to the vapor that would only scale with the interfacial area, whereas the liquid interfacial heat source scales with multiple properties (phase velocity, density, etc.). This may cause a situation where the vapor absorbs less heat than what actually occurs, with the liquid absorbing more heat. This would cause the mismatch in liquid and vapor enthalpy, thus leading to a higher liquid temperature. However, this method of dealing with interfacial vapor heat transfer is not unheard of. Both RELAP-5 and TRACE [6] use the exact same model for interfacial vapor heat transfer.

6.3 Two-Phase Wall Drag and Mass Flux

The pressure drop due to wall drag is completely allocated to the liquid phase under a normal flow regime in CTF. The pressure differential with respect to the axial position for both phases (k) is calculated from:

$$\frac{\partial P}{\partial z}\Big|_{fric,k} = \frac{f_w G_k^2}{2 D_e \rho_l} \Phi^2 \tag{6.65}$$

With the two-phase multiplier being defined for the normal flow regime as:

$$\Phi^2 = \frac{1}{\alpha_l^2} \tag{6.66}$$

For normal (Tw<Tchf) flow regimes, all of the wall drag is partitioned to the liquid phase. Under these conditions, and with the use of the two-phase multiplier, the pressure derivative for the liquid phase reduces to:

$$\frac{\partial P}{\partial z}\Big|_{fric,l} = \frac{f_w(\rho_l v_l)^2}{2D_e\rho_l} \tag{6.67}$$

This shows no additional wall drag force imposed from the addition of the vapor phase being generated at the wall. Thus, the pressure drop across each cell is calculated almost identically to its previous single-phase calculation, with no partitioning occurring to the vapor phase. While this may be valid for an annular flow regime, it is inappropriate for other flow conditions. This reduction in wall drag during two-phase conditions would lead to a reduced pressure drop along the axial length. The result of this would be a less significant drop in the mass flux over the axial length, as wall drag is not impeding fluid flow to a full effect. This effect may have caused the significantly higher mass flux values that were observed in the 17x17 evaluations.

RELAP-5 and TRACE use a similar approach, however there is a more accurate account of the two-phase behavior. This occurs through the use of more advanced two-phase multipliers and wall drag partitioning schemes. TRACE does utilize a two-phase multiplier that is identical to the one found in CTF, however it is only used in the case of annular flow. For the bubbly flow regime, a multiplier is constructed which has a similar form:

$$\Phi_l^2 = \frac{1}{\alpha_l^{1.72}} \tag{6.68}$$

RELAP-5 takes a different approach for the two-phase multiplier. Instead of using void fraction, the multiplier is determined from the Lockhart-Martinelli parameter. It takes the following form:

$$\Phi_l^2 = 1 + \frac{C}{\chi} + \frac{1}{\chi^2} \tag{6.69}$$

Where,

$$C = -2 + f_1(G)T_1(\Lambda, \mathrm{G}) \tag{6.70}$$

$$f_1(G) = 28 - 0.3\sqrt{G} \tag{6.71}$$

$$T_1(\Lambda, G) = \exp\left[\frac{(-log_{10}\Lambda + 2.5)^2}{2.4 - G * 10^{-4}}\right] \tag{6.72}$$

$$\Lambda = \frac{\rho_g}{\rho_f}\left(\frac{\mu_f}{\mu_g}\right)^{0.2} \tag{6.73}$$

$$\chi = \frac{\dot{m}_l}{\dot{m}_v}\sqrt{\frac{\rho_v}{\rho_l}} \tag{6.74}$$

TRACE uses the exact partitioning scheme for wall drag that CTF utilizes. Under the pre-CHF flow regimes (bubbly, annular/mist) all of the wall drag is partitioned to the liquid phase. RELAP-5 applies a more sophisticated method that is derived from a quasi-steady form of the momentum equation. Upon simplification of the quasi-steady form, the partitioning occurs as:

$$\tau_l P_{wl} = \alpha_l \left(\frac{\partial P}{\partial x}|_{2\Phi}\right)\left(\frac{Z^2}{\alpha_v + \alpha_l Z^2}\right) \tag{6.75}$$

$$\alpha_v P_{wv} = \alpha_v \left(\frac{\partial P}{\partial x}|_{2\Phi}\right)\left(\frac{Z^2}{\alpha_v + \alpha_l Z^2}\right) \tag{6.76}$$

Where,

$$Z^2 = \frac{f_l \rho_l v_l^2 \left(\frac{\alpha_{lw}}{\alpha_l}\right)}{f_v \rho_v v_v^2 \left(\frac{\alpha_{vw}}{\alpha_v}\right)} \tag{6.77}$$

$$\alpha_{lw} = liquid\ volume\ fraction\ on\ the\ wall$$

COBRA-EN has three options for two-phase multipliers. These three options more accurately account for the effect of vapor on wall drag. They are shown below:

0. Homogeneous Multiplier

$$\Phi^2 = \frac{\rho_l}{\rho_{mix}}\left[\frac{\mu_f}{x\mu_g + (1-x)\mu_f}\right]^b \tag{6.78}$$

1. Armand Correlation

$$\Phi^2 = \begin{bmatrix} \frac{(1-x)^2}{(1-\alpha)^{1.42}} & if\ 0 < \alpha < 0.6 \\ 0.478\frac{(1-x)^2}{(1-\alpha)^{2.2}} & if\ 0.6 < \alpha < 0.9 \\ 1.73\frac{(1-x)^2}{(1-\alpha)^{1.64}} & if 0.9 < \alpha < 1.0 \end{bmatrix} \tag{6.79}$$

2. EPRI Correlation

$$\Phi^2 = 1.0 + \left(\frac{\nu_g}{\nu_f} - 1\right) x C_f \tag{6.80}$$

$$C_f = 1.02x^{-0.175}(0.0036G)^{-0.45}\ if\ P \geq 600\ psi \tag{6.81}$$

$$C_f = 0.357x^{-0.175}(0.0036G)^{-0.45}\left(1 + 10\frac{P}{P_c}\right)\ if\ P < 600\ psi \tag{6.82}$$

7. Conclusion and Future Work

7.1 Conclusion

COBRA-TF was found to be an accurate predictor of some of the flow quantities analyzed in this study. The experimental data utilized allowed for a basis of comparison between fluid temperature, wall temperature, mass flux and enthalpy for individual channels in 4x4 and 5x5 bundles. The Castellana 4x4 cases assisted with comparisons in bundle-averaged enthalpy, channel specific enthalpy and mass flux. CTF accurately evaluated the bundle-averaged enthalpy, while disparities occurred between the channel specific enthalpy and mass flux for both cases. However, the calculated mass flux in CTF was a better predictor of the true exit mass flux when compared to the values produced in COBRA-EN.

The EPRI 5x5 cases brought a significant issue forward with regards to CTF. The wall temperature calculation in COBRA-TF was drastically higher than the experimental or COBRA-EN calculated values. Upon further analysis, this was found to be due to an invalid heat transfer correlation being utilized for most given operating conditions. In addition, there was slight variation in the liquid phase temperature distribution that was observed following transition from single-phase to two-phase conditions. The partitioning of the liquid and vapor enthalpy would be a root cause of this error. This could occur through a mismatched heat input to each of these phases. The wall heat transfer partitioning and interfacial heat transfer was mentioned as a source of this inaccurate enthalpy partitioning effect. While very little can be assessed about the flow quality and void fractions based on the experimental data, the comparisons with COBRA-EN were valuable. For the cases analyzed, CTF produced distributions that were not dissimilar from those calculated in COBRA-EN. The main difference noted was some nominal void fraction that existed earlier in the channel in CTF. This was found to result from a minimum void fraction setting of 10^{-6}.

Finally, the standard 17x17 mixing model and conduction solution comparisons allowed for an assessment of some user specified options. For normal operating conditions, the increased spatial dimensionality had little effect on the heat transfer solution. In addition, the modification of the turbulent mixing model varied the channel specific enthalpy only slightly. This portion of the study did display a large disparity in the channel mass flux that

occurs between the two codes. COBRA-TF predicts a distribution that did not display the effects of spacer grids and whose magnitude was significantly higher than the one found in COBRA-EN. The modification of the turbulent mixing model did very little to alleviate this issue. Upon analyzing the two-phase pressure drop calculation, it was found that the method for calculating the wall drag component does not accurately represent the physics. This leads to a lower prediction of the pressure drop, which results in a higher mass flux in the channel.

7.2 Future Work and Recommendations

The test cases presented a wide variety of issues that are occurring in COBRA-TF for the simulation of subcooled boiling conditions of interest to normal operation of Pressurized Water Reactors. The over prediction of the wall temperature is the most significant issue that was noticed. To alleviate this, other more valid heat transfer correlations could be implemented. This could further be improved by allowing this implementation to shift between heat transfer correlations based on the current flow conditions.

The inaccurate physics that were noted should be investigated further. The skewing of the fluid temperature profile upon transition to a two-phase fluid was noted to result from an incorrect partitioning of the enthalpy to each phase. From this, an assessment was made based on the heat input to each phase due to wall heat transfer and interfacial heat transfer. These may not be affecting the fluid temperature to such a large degree, and a more in depth study would be required to validate these claims. In addition, the mass flux distribution in the 17x17 was a concern. The inaccurate representation of the spacer and relatively unchanged magnitude of the mass flux over the channel length require attention.

Finally, these cases were only analyzed for conditions indicative of a pressurized water reactor. The code must be assessed completely for boiling water reactors, which operate with a lower pressure and lower heat flux. Due to this, more robust boiling regimes can exist. CTF's performance must be assessed in order to ensure that accurate predictions occur for these differing flow regimes and heat transfer mechanisms.

Bibliography:

[1] Avramova M. N. and Salko R. K. "CTF Theory Manual." Pennsylvania State University, Department of Mechanical and Nuclear Engineering. 2013.

[2] D. Basile, M. Beghi, R. Chierici, E. Salina and E. Brega. "COBRA-EN, An upgraded version of the COBRA-3C/MIT code for thermal-hydraulic transient analysis of light water reactor fuel assemblies and cores." Radiation Safety Information Computational Center, Oak Ridge National Lab. 1999.

[3] Subcooled Boiling Data From Rod Bundles, EPRI, Palo Alto, CA; 2002. 1003383.

[4] Castellana F. S. and Casterline J. E. "Subchannel flow and enthalpy distributions at the exit of a typical nuclear fuel core geometry." *Nuclear Engineering and Design,* vol. 22, no. 1, pp. 3-18. 1972.

[5] McGuire Nuclear Station UFSAR. 2003.

[6] TRACE V5.0 Theory Manual. "Field Equations, Solution Methods and Physical Models." US NRC, Washington DC.

[7] RELAP-5 3D Code Manual. "Volume 1: Code Structure, System Models and Solution Methods." Idaho National Engineering and Environmental Laboratory, Idaho Falls.

[8] Chen J. C. "Correlation for Boiling Heat Transfer to Saturated Fluids in Convective Flow." *I & EC Process Design and Development,* vol. 5, no. 3, pp. 322-329. 1966.

[9] Wagner W. and Prub A. "The IAPWS Formulation 1995 for the Thermodynamic Properties of Ordinary Water Substance for General and Scientific Use." *Journal of Physical and Chemical Reference Data,* 31, 387. 2002

[10] F. S. Castellana, W. T. Adams, and J. E. Casterline. “Single-phase subchannel mixing in a simulated nuclear fuel assembly.” *Nuclear Engineering and Design*, vol. 26, no. 2, pp. 242-249. 1974.

Appendix

Appendix A: COBRA-TF and COBRA_EN Mixing Models

A.1 COBRA-TF Mixing Models:

The turbulent exchange of momentum per unit length is defined by:

$$w_{ij}^{'M} = V_{ij}^{T}\left(G_{iz} - G_{jz}\right)s_k\Delta x \tag{A.1}$$

Turbulent exchanges of the remaining conserved quantities are calculated by simply replacing the conserved quantity in the equation.

$$w_{ij}^{'E} = V_{ij}^{T}\left(\rho_i h_i - \rho_j h_j\right)s_k\Delta x \tag{A.2}$$

$$w_{ij}^{'D} = V_{ij}^{T}\left(\rho_i - \rho_j\right)s_k\Delta x \tag{A.3}$$

The transverse velocity is defined as:

$$V_{ij}^{T} = \frac{\beta_{\mathrm{tp}}\,\overline{\mathrm{G}}}{\overline{\rho}_{\mathrm{mix}}} \tag{A.4}$$

The differences in mixing found in CTF are due to specification of the mixing coefficient, β.

Default:

$$\beta_{sp} = 0.5\lambda Re^{-0.1}\left[1 + \left(\frac{D_{h,jj}}{D_{h,ii}}\right)^{1.5}\right]\left(\frac{D_{h,ii}}{D_{rod}}\right) \;\; if\; D_{h,ii} < D_{h,jj} \tag{A.5}$$

$$\beta_{sp} = 0.5\lambda Re^{-0.1}\left[1 + \left(\frac{D_{h,ii}}{D_{h,jj}}\right)^{1.5}\right]\left(\frac{D_{h,jj}}{D_{rod}}\right) \;\; if\; D_{h,jj} < D_{h,ii} \tag{A.6}$$

$$\lambda = 0.0058\left(\frac{s_k}{D_{rod}}\right)^{-1.46} \tag{A.7}$$

$$\beta_{tp} = 1 + \left(\beta_{tp,M} - 1\right)\left(\frac{x}{x_m}\right), \qquad if\; x < x_M \tag{A.8}$$

$$\beta_{tp} = 1 + \left(\beta_{tp,M} - 1\right)\left(\frac{x_M - x_0}{x - x_0}\right), \qquad if\; x > x_M \tag{A.9}$$

Where,

$$\beta_{tp,M} = \beta_{sp}\Theta_M \tag{A.10}$$

$$x = \frac{\dot{m}_v}{\dot{m}_v + \dot{m}_l + \dot{m}_e} \tag{A.11}$$

$$x_M = \frac{\frac{0.4\left[\rho_f(\rho_f - \rho_g)gD_h\right]^{1.2}}{G} + 0.6}{\left(\frac{\rho_f}{\rho_g}\right)^{\frac{1}{2}} + 0.6} \tag{A.12}$$

$$x_0 = 0.75 x_M Re^{0.0417} \tag{A.13}$$

*Note: For the given simulations, Θ_M was set to 1.0.

Secondary Option:

Instead of allowing CTF to calculate the coefficient via the previous correlation, the user may choose to manually define a two-phase mixing coefficient.

Void Drift Cross-flow:

The void drift cross-flow is calculated in a similar manner to the turbulent mixing cross-flow. The cross-flow per unit length of each conserved quantity is given by:

$$w_{ij}^{'M} = -V_{ij}^T(G_i + G_j)(\alpha_i - \alpha_j)_{equil} s_k \Delta x \tag{A.14}$$

$$w_{ij}^{'E} = -V_{ij}^T(\alpha_i\rho_i h_i + \alpha_j\rho_j h_j)(\alpha_i - \alpha_j)_{equil} s_k \Delta x \tag{A.15}$$

$$w_{ij}^{'D} = -V_{ij}^T(\alpha_i\rho_i + \alpha_j\rho_j)(\alpha_i - \alpha_j)_{equil} s_k \Delta x \tag{A.16}$$

Where,

$$(\alpha_i - \alpha_j)_{equil} = \frac{K_a(G_i - G_j)}{\bar{G}} \tag{A.17}$$

A.2 COBRA-EN Mixing Models:

There are four separate mixing models that the user may choose in COBRA-EN. They are shown in equations A.18, A.19, A.20 and A.21.

1.
$$w_k' = a(Re_k)^b \left(\frac{s_k}{l_k}\right) D_k G_k \qquad (A.18)$$

2.
$$w_k' = a(Re_k)^b D_k G_k \qquad (A.19)$$

3.
$$w_k' = a(Re_k)^b s_k G_k \qquad (A.20)$$

4.
$$w_k' = a s_k G_k \qquad (A.21)$$

The exponent, b, and the coefficient, a, given in each of these equations were set according to Castellana et. al [10]. These coefficients are defined by equating the mixing model to the following equation:

$$\beta = 0.0071 \left(\frac{D_k}{s_k}\right) Re^{-0.10} \qquad (A.22)$$

where the cross-flow per unit length given in the mixing model may be converted to a mixing coefficient as:

$$w' = \beta \bar{G} s \qquad (A.23)$$

Appendix B: Sample Input Deck for 5x5

```
**********************************************************************
**********
*MAIN CONTROL DATA
**********************************************************************
**********
*ICOBRA
     1
*INITIAL   DUMPF
      1      0
**    EPSO    OITMAX    IITMAX
  0.001000         5        40
*TITLE
Simple
**********************************************************************
**********
*GROUP 1 - Calculation Variables and Initial Conditions                 *
**********************************************************************
**********
**NGR
  1
**NGAS IRFC EDMD IMIX ISOL       GINIT NOTRN MESH NDM9 NM10 NM11 NM12
NM13 NM14
    1    2    0    2    3  0.1050E+02     1    1    0    0    0    0    0    0
*Card 1.2
**         GTOT          AFLUX         DHFRAC
  0.1049906E+02  0.624569E+02  0.0000000E+00
*Card 1.3
**         PREF           HIN          HGIN         VFRAC1         VFRAC2
   155.4078290   1312.3307750    288.4200000      1.0000000      0.9999000
*Card 1.4
**GTP(1)   VFRAC(3)  GTP(2) VFRAC(4)  GTP(3) VFRAC(5)  GTP(4) VFRAC(6)
    air     0.0001
**********************************************************************
**********
*GROUP 2 - Channel Description                                          *
**********************************************************************
**********
**NGR
   2
*Card 2.1
**  NCH NDM2 NDM3 NDM4 NDM5 NDM6 NDM7 NDM8 NDM9 NM10 NM11 NM12
```

NM13 NM14

36 0 0 0 0 0 0 0 0 0 0 0 0 0
*Card 2.2
** I AN PW ABOT ATOP NMGP X Y XSIZ YSIZ
1 0.52201E-04 0.87776E-02 0 0 0 0.42545E-02 0.45085E-02 0.85090E-02 0.90170E-02
2 0.76305E-04 0.17555E-01 0 0 0 0.19241E-01 0.45085E-02 0.14986E-01 0.90170E-02
3 0.76305E-04 0.17555E-01 0 0 0 0.34226E-01 0.45085E-02 0.14986E-01 0.90170E-02
4 0.76305E-04 0.17555E-01 0 0 0 0.49213E-01 0.45085E-02 0.14986E-01 0.90170E-02
5 0.76305E-04 0.17555E-01 0 0 0 0.64199E-01 0.45085E-02 0.14986E-01 0.90170E-02
6 0.52201E-04 0.87776E-02 0 0 0 0.79185E-01 0.45085E-02 0.85090E-02 0.90170E-02
7 0.86080E-04 0.17555E-01 0 0 0 0.42545E-02 0.19241E-01 0.85090E-02 0.14732E-01
8 0.12268E-03 0.35110E-01 0 0 0 0.19241E-01 0.19241E-01 0.14986E-01 0.14732E-01
9 0.12268E-03 0.35110E-01 0 0 0 0.34226E-01 0.19241E-01 0.14986E-01 0.14732E-01
10 0.12268E-03 0.35110E-01 0 0 0 0.49213E-01 0.19241E-01 0.14986E-01 0.14732E-01
11 0.12268E-03 0.35110E-01 0 0 0 0.64199E-01 0.19241E-01 0.14986E-01 0.14732E-01
12 0.86080E-04 0.17555E-01 0 0 0 0.79185E-01 0.19241E-01 0.85090E-02 0.14732E-01
13 0.86080E-04 0.17555E-01 0 0 0 0.42545E-02 0.33973E-01 0.85090E-02 0.14732E-01
14 0.12268E-03 0.35110E-01 0 0 0 0.19241E-01 0.33973E-01 0.14986E-01 0.14732E-01
15 0.12268E-03 0.35110E-01 0 0 0 0.34226E-01 0.33973E-01 0.14986E-01 0.14732E-01
16 0.12268E-03 0.35110E-01 0 0 0 0.49213E-01 0.33973E-01 0.14986E-01 0.14732E-01
17 0.12268E-03 0.35110E-01 0 0 0 0.64199E-01 0.33973E-01 0.14986E-01 0.14732E-01
18 0.86080E-04 0.17555E-01 0 0 0 0.79185E-01 0.33973E-01 0.85090E-02 0.14732E-01
19 0.86080E-04 0.17555E-01 0 0 0 0.42545E-02 0.48705E-01 0.85090E-02 0.14732E-01

20 0.12268E-03 0.35110E-01 0 0 0 0.19241E-01 0.48705E-01 0.14986E-01 0.14732E-01
21 0.12268E-03 0.35110E-01 0 0 0 0.34226E-01 0.48705E-01 0.14986E-01 0.14732E-01
22 0.12268E-03 0.35110E-01 0 0 0 0.49213E-01 0.48705E-01 0.14986E-01 0.14732E-01
23 0.12268E-03 0.35110E-01 0 0 0 0.64199E-01 0.48705E-01 0.14986E-01 0.14732E-01
24 0.86080E-04 0.17555E-01 0 0 0 0.79185E-01 0.48705E-01 0.85090E-02 0.14732E-01
25 0.86080E-04 0.17555E-01 0 0 0 0.42545E-02 0.63437E-01 0.85090E-02 0.14732E-01
26 0.12268E-03 0.35110E-01 0 0 0 0.19241E-01 0.63437E-01 0.14986E-01 0.14732E-01
27 0.12268E-03 0.35110E-01 0 0 0 0.34226E-01 0.63437E-01 0.14986E-01 0.14732E-01
28 0.12268E-03 0.35110E-01 0 0 0 0.49213E-01 0.63437E-01 0.14986E-01 0.14732E-01
29 0.12268E-03 0.35110E-01 0 0 0 0.64199E-01 0.63437E-01 0.14986E-01 0.14732E-01
30 0.86080E-04 0.17555E-01 0 0 0 0.79185E-01 0.63437E-01 0.85090E-02 0.14732E-01
31 0.52201E-04 0.87776E-02 0 0 0 0.42545E-02 0.78168E-01 0.85090E-02 0.90170E-02
32 0.76305E-04 0.17555E-01 0 0 0 0.19241E-01 0.78168E-01 0.14986E-01 0.90170E-02
33 0.76305E-04 0.17555E-01 0 0 0 0.34226E-01 0.78168E-01 0.14986E-01 0.90170E-02
34 0.76305E-04 0.17555E-01 0 0 0 0.49213E-01 0.78168E-01 0.14986E-01 0.90170E-02
35 0.76305E-04 0.17555E-01 0 0 0 0.64199E-01 0.78168E-01 0.14986E-01 0.90170E-02
36 0.52201E-04 0.87776E-02 0 0 0 0.79185E-01 0.78168E-01 0.85090E-02 0.90170E-02
****
*GROUP 3 - Transverse Channel Connection (Gap) Data
****
**NGR
3
*Card 3.1

```
**  NK NDM2 NDM3 NDM4 NDM5 NDM6 NDM7 NDM8 NDM9 NM10 NM11 NM12
NM13 NM14
   60   0   0   0   0   0   0   0   0   0   0   0   0   0
*Card 3.2
**   K    IK    JK       GAP       LNGT  WKR FWAL IGPB IGPA FACT IGAP JGAP IGAP

JGAP IGAP JGAP
*Card 3.3
**GMULT   ETNR
    1    1    2 0.343E-02 0.150E-01 0.5 0.0   0   0 1.0   0   0   0   0   0   0
     1   0.0
    2    1    7 0.330E-02 0.147E-01 0.5 0.0   0   0 1.0   0   0   0   0   0   0
     1   0.0
    3    2    3 0.343E-02 0.150E-01 0.5 0.0   0   0 1.0   0   0   0   0   0   0
     1   0.0
    4    2    8 0.381E-02 0.147E-01 0.5 0.0   0   0 1.0   0   0   0   0   0   0
     1   0.0
    5    3    9 0.381E-02 0.147E-01 0.5 0.0   0   0 1.0   0   0   0   0   0   0
     1   0.0
    6    3    4 0.343E-02 0.150E-01 0.5 0.0   0   0 1.0   0   0   0   0   0   0
     1   0.0
    7    4   10 0.381E-02 0.147E-01 0.5 0.0   0   0 1.0   0   0   0   0   0   0
     1   0.0
    8    4    5 0.343E-02 0.150E-01 0.5 0.0   0   0 1.0   0   0   0   0   0   0
     1   0.0
    9    5   11 0.381E-02 0.147E-01 0.5 0.0   0   0 1.0   0   0   0   0   0   0
     1   0.0
   10    5    6 0.343E-02 0.150E-01 0.5 0.0   0   0 1.0   0   0   0   0   0   0
     1   0.0
   11    6   12 0.330E-02 0.147E-01 0.5 0.0   0   0 1.0   0   0   0   0   0   0
     1   0.0
   12    7   13 0.330E-02 0.147E-01 0.5 0.0   0   0 1.0   0   0   0   0   0   0
     1   0.0
   13    7    8 0.356E-02 0.150E-01 0.5 0.0   0   0 1.0   0   0   0   0   0   0
     1   0.0
   14    8    9 0.356E-02 0.144E-01 0.5 0.0   0   0 1.0   0   0   0   0   0   0
     1   0.0
   15    8   14 0.381E-02 0.147E-01 0.5 0.0   0   0 1.0   0   0   0   0   0   0
     1   0.0
   16    9   15 0.381E-02 0.147E-01 0.5 0.0   0   0 1.0   0   0   0   0   0   0
     1   0.0
   17    9   10 0.356E-02 0.150E-01 0.5 0.0   0   0 1.0   0   0   0   0   0   0
     1   0.0
```

```
 18   10   11  0.356E-02  0.150E-01  0.5  0.0   0   0  1.0   0   0   0   0   0   0
  1   0.0
 19   10   16  0.381E-02  0.147E-01  0.5  0.0   0   0  1.0   0   0   0   0   0   0
  1   0.0
 20   11   17  0.381E-02  0.147E-01  0.5  0.0   0   0  1.0   0   0   0   0   0   0
  1   0.0
 21   11   12  0.356E-02  0.150E-01  0.5  0.0   0   0  1.0   0   0   0   0   0   0

1   0.0
 22   12   18  0.330E-02  0.147E-01  0.5  0.0   0   0  1.0   0   0   0   0   0   0
  1   0.0
 23   13   19  0.330E-02  0.147E-01  0.5  0.0   0   0  1.0   0   0   0   0   0   0
  1   0.0
 24   13   14  0.356E-02  0.150E-01  0.5  0.0   0   0  1.0   0   0   0   0   0   0
  1   0.0
 25   14   15  0.356E-02  0.150E-01  0.5  0.0   0   0  1.0   0   0   0   0   0   0
  1   0.0
 26   14   20  0.381E-02  0.147E-01  0.5  0.0   0   0  1.0   0   0   0   0   0   0
  1   0.0
 27   15   16  0.356E-02  0.150E-01  0.5  0.0   0   0  1.0   0   0   0   0   0   0
  1   0.0
 28   15   21  0.381E-02  0.147E-01  0.5  0.0   0   0  1.0   0   0   0   0   0   0
  1   0.0
 29   16   22  0.381E-02  0.147E-01  0.5  0.0   0   0  1.0   0   0   0   0   0   0
  1   0.0
 30   16   17  0.356E-02  0.150E-01  0.5  0.0   0   0  1.0   0   0   0   0   0   0
  1   0.0
 31   17   23  0.381E-02  0.147E-01  0.5  0.0   0   0  1.0   0   0   0   0   0   0
  1   0.0
 32   17   18  0.356E-02  0.150E-01  0.5  0.0   0   0  1.0   0   0   0   0   0   0
  1   0.0
 33   18   24  0.330E-02  0.147E-01  0.5  0.0   0   0  1.0   0   0   0   0   0   0
  1   0.0
 34   19   20  0.356E-02  0.150E-01  0.5  0.0   0   0  1.0   0   0   0   0   0   0
  1   0.0
 35   19   25  0.330E-02  0.147E-01  0.5  0.0   0   0  1.0   0   0   0   0   0   0
  1   0.0
 36   20   21  0.356E-02  0.150E-01  0.5  0.0   0   0  1.0   0   0   0   0   0   0
  1   0.0
 37   20   26  0.381E-02  0.147E-01  0.5  0.0   0   0  1.0   0   0   0   0   0   0
  1   0.0
 38   21   22  0.356E-02  0.150E-01  0.5  0.0   0   0  1.0   0   0   0   0   0   0
  1   0.0
```

```
  39   21   27  0.381E-02  0.147E-01  0.5  0.0   0   0  1.0   0   0   0   0   0   0
   1   0.0
  40   22   28  0.381E-02  0.147E-01  0.5  0.0   0   0  1.0   0   0   0   0   0   0
   1   0.0
  41   22   23  0.356E-02  0.150E-01  0.5  0.0   0   0  1.0   0   0   0   0   0   0
   1   0.0
  42   23   29  0.381E-02  0.147E-01  0.5  0.0   0   0  1.0   0   0   0   0   0   0
   1   0.0
  43   23   24  0.356E-02  0.150E-01  0.5  0.0   0   0  1.0   0   0   0   0   0   0

1   0.0
  44   24   30  0.330E-02  0.147E-01  0.5  0.0   0   0  1.0   0   0   0   0   0   0
   1   0.0
  45   25   31  0.330E-02  0.147E-01  0.5  0.0   0   0  1.0   0   0   0   0   0   0
   1   0.0
  46   25   26  0.356E-02  0.150E-01  0.5  0.0   0   0  1.0   0   0   0   0   0   0
   1   0.0
  47   26   27  0.356E-02  0.150E-01  0.5  0.0   0   0  1.0   0   0   0   0   0   0
   1   0.0
  48   26   32  0.381E-02  0.147E-01  0.5  0.0   0   0  1.0   0   0   0   0   0   0
   1   0.0
  49   27   28  0.356E-02  0.150E-01  0.5  0.0   0   0  1.0   0   0   0   0   0   0
   1   0.0
  50   27   33  0.381E-02  0.147E-01  0.5  0.0   0   0  1.0   0   0   0   0   0   0
   1   0.0
  51   28   29  0.356E-02  0.150E-01  0.5  0.0   0   0  1.0   0   0   0   0   0   0
   1   0.0
  52   28   34  0.381E-02  0.147E-01  0.5  0.0   0   0  1.0   0   0   0   0   0   0
   1   0.0
  53   29   35  0.381E-02  0.147E-01  0.5  0.0   0   0  1.0   0   0   0   0   0   0
   1   0.0
  54   29   30  0.356E-02  0.150E-01  0.5  0.0   0   0  1.0   0   0   0   0   0   0
   1   0.0
  55   30   36  0.330E-02  0.147E-01  0.5  0.0   0   0  1.0   0   0   0   0   0   0
   1   0.0
  56   31   32  0.343E-02  0.150E-01  0.5  0.0   0   0  1.0   0   0   0   0   0   0
   1   0.0
  57   32   33  0.343E-02  0.150E-01  0.5  0.0   0   0  1.0   0   0   0   0   0   0
   1   0.0
  58   33   34  0.343E-02  0.150E-01  0.5  0.0   0   0  1.0   0   0   0   0   0   0
   1   0.0
  59   34   35  0.343E-02  0.150E-01  0.5  0.0   0   0  1.0   0   0   0   0   0   0
   1   0.0
```

```
   60    35    36  0.343E-02  0.150E-01  0.5  0.0    0    0  1.0    0    0    0    0    0    0
    1    0.0
*Card 3.3.5
**   K          X          Y      NORM
    1 0.11748E-01 0.45085E-02     x
    2 0.42545E-02 0.11875E-01     y
    3 0.26733E-01 0.45085E-02     x
    4 0.19241E-01 0.11875E-01     y
    5 0.34226E-01 0.11875E-01     y
    6 0.41719E-01 0.45085E-02     x
    7 0.49213E-01 0.11875E-01     y

    8 0.56706E-01 0.45085E-02     x
    9 0.64199E-01 0.11875E-01     y
   10 0.71691E-01 0.45085E-02     x
   11 0.79185E-01 0.11875E-01     y
   12 0.42545E-02 0.26607E-01     y
   13 0.11748E-01 0.19241E-01     x
   14 0.26733E-01 0.19241E-01     x
   15 0.19241E-01 0.26607E-01     y
   16 0.34226E-01 0.26607E-01     y
   17 0.41719E-01 0.19241E-01     x
   18 0.56706E-01 0.19241E-01     x
   19 0.49213E-01 0.26607E-01     y
   20 0.64199E-01 0.26607E-01     y
   21 0.71691E-01 0.19241E-01     x
   22 0.79185E-01 0.26607E-01     y
   23 0.42545E-02 0.41339E-01     y
   24 0.11748E-01 0.33973E-01     x
   25 0.26733E-01 0.33973E-01     x
   26 0.19241E-01 0.41339E-01     y
   27 0.41719E-01 0.33973E-01     x
   28 0.34226E-01 0.41339E-01     y
   29 0.49213E-01 0.41339E-01     y
   30 0.56706E-01 0.33973E-01     x
   31 0.64199E-01 0.41339E-01     y
   32 0.71691E-01 0.33973E-01     x
   33 0.79185E-01 0.41339E-01     y
   34 0.11748E-01 0.48705E-01     x
   35 0.42545E-02 0.56070E-01     y
   36 0.26733E-01 0.48705E-01     x
   37 0.19241E-01 0.56070E-01     y
   38 0.41719E-01 0.48705E-01     x
```

```
   39 0.34226E-01 0.56070E-01    y
   40 0.49213E-01 0.56070E-01    y
   41 0.56706E-01 0.48705E-01    x
   42 0.64199E-01 0.56070E-01    y
   43 0.71691E-01 0.48705E-01    x
   44 0.79185E-01 0.56070E-01    y
   45 0.42545E-02 0.70802E-01    y
   46 0.11748E-01 0.63437E-01    x
   47 0.26733E-01 0.63437E-01    x
   48 0.19241E-01 0.70802E-01    y
   49 0.41719E-01 0.63437E-01    x
   50 0.34226E-01 0.70802E-01    y
   51 0.56706E-01 0.63437E-01    x

 52 0.49213E-01 0.70802E-01    y
   53 0.64199E-01 0.70802E-01    y
   54 0.71691E-01 0.63437E-01    x
   55 0.79185E-01 0.70802E-01    y
   56 0.11748E-01 0.78168E-01    x
   57 0.26733E-01 0.78168E-01    x
   58 0.41719E-01 0.78168E-01    x
   59 0.56706E-01 0.78168E-01    x
   60 0.71691E-01 0.78168E-01    x
*Card 3.4
**NLGP
    0
*************************************************************************
********************
*GROUP 4 - Vertical Channel Connection Data                              *
*************************************************************************
********************
**NGR
   4
*Card 4.1
**NSEC NSIM IREB NDM4 NDM5 NDM6 NDM7 NDM8 NDM9 NM10 NM11 NM12
NM13 NM14
    1   1   0   0   0   0   0   0   0   0   0   0   0   0
*Card 4.2
**ISEC    NCHN  NONO       DXS     IVAR
    1      36    20 0.10668E+00       5
*Card 4.3
**JLEV      VARDX  JLEV      VARDX  JLEV      VARDX  JLEV      VARDX  JLEV
VARDX
```

5 0.10668E+00 9 0.10668E+00 13 0.10668E+00 17 0.10668E+00 21 0.10668E+00

*Card 4.4

** I KCHA KCHA KCHA KCHA KCHA KCHA KCHB KCHB KCHB KCHB KCHB KCHB

1	1	0	0	0	0	0	1	0	0	0	0	0
2	2	0	0	0	0	0	2	0	0	0	0	0
3	3	0	0	0	0	0	3	0	0	0	0	0
4	4	0	0	0	0	0	4	0	0	0	0	0
5	5	0	0	0	0	0	5	0	0	0	0	0
6	6	0	0	0	0	0	6	0	0	0	0	0
7	7	0	0	0	0	0	7	0	0	0	0	0
8	8	0	0	0	0	0	8	0	0	0	0	0
9	9	0	0	0	0	0	9	0	0	0	0	0
10	10	0	0	0	0	0	10	0	0	0	0	0
11	11	0	0	0	0	0	11	0	0	0	0	0
12	12	0	0	0	0	0	12	0	0	0	0	0
13	13	0	0	0	0	0	13	0	0	0	0	0
14	14	0	0	0	0	0	14	0	0	0	0	0
15	15	0	0	0	0	0	15	0	0	0	0	0
16	16	0	0	0	0	0	16	0	0	0	0	0
17	17	0	0	0	0	0	17	0	0	0	0	0
18	18	0	0	0	0	0	18	0	0	0	0	0
19	19	0	0	0	0	0	19	0	0	0	0	0
20	20	0	0	0	0	0	20	0	0	0	0	0
21	21	0	0	0	0	0	21	0	0	0	0	0
22	22	0	0	0	0	0	22	0	0	0	0	0
23	23	0	0	0	0	0	23	0	0	0	0	0
24	24	0	0	0	0	0	24	0	0	0	0	0
25	25	0	0	0	0	0	25	0	0	0	0	0
26	26	0	0	0	0	0	26	0	0	0	0	0
27	27	0	0	0	0	0	27	0	0	0	0	0
28	28	0	0	0	0	0	28	0	0	0	0	0
29	29	0	0	0	0	0	29	0	0	0	0	0
30	30	0	0	0	0	0	30	0	0	0	0	0
31	31	0	0	0	0	0	31	0	0	0	0	0
32	32	0	0	0	0	0	32	0	0	0	0	0
33	33	0	0	0	0	0	33	0	0	0	0	0
34	34	0	0	0	0	0	34	0	0	0	0	0
35	35	0	0	0	0	0	35	0	0	0	0	0
36	36	0	0	0	0	0	36	0	0	0	0	0

*Card4.5

```
** IWDE
     36
*Card 4.6
** MSIM
    720
*******************************************************************************
********************
*GROUP 7 - Grid Loss Coefficient Data                                          *
*******************************************************************************
********************
**NGR
   7
*Card 7.1
** NCD NGT  IFGQF IFSDRP  IFESPV  IFTPE  IGTEMP  NFBS  NDM9 NDM10
NDM11 NDM12 NDM13 NDM14
    15  0     0     0      0     0      0    0    0    0    0    0    0    0
*Card 7.2

**  CDL    J   CD1   CD2   CD3   CD4   CD5   CD6   CD7   CD8   CD9  CD10  CD11
CD12
 0.41100   2    1    2    3    4    5    6    7    8    9   10    11    12
 0.41100   2   13   14   15   16   17   18   19   20   21   22   23   24
 0.41100   2   25   26   27   28   29   30   31   32   33   34   35   36
 0.41100   6    1    2    3    4    5    6    7    8    9   10    11    12
 0.41100   6   13   14   15   16   17   18   19   20   21   22   23   24
 0.41100   6   25   26   27   28   29   30   31   32   33   34   35   36
 0.41100  11    1    2    3    4    5    6    7    8    9   10    11    12
 0.41100  11   13   14   15   16   17   18   19   20   21   22   23   24
 0.41100  11   25   26   27   28   29   30   31   32   33   34   35   36
 0.41100  15    1    2    3    4    5    6    7    8    9   10    11    12
 0.41100  15   13   14   15   16   17   18   19   20   21   22   23   24
 0.41100  15   25   26   27   28   29   30   31   32   33   34   35   36
 0.41100  19    1    2    3    4    5    6    7    8    9   10    11    12
 0.41100  19   13   14   15   16   17   18   19   20   21   22   23   24
 0.41100  19   25   26   27   28   29   30   31   32   33   34   35   36
*******************************************************************************
********************
*GROUP 8 - Rod and Unheated Conductor Data                                     *
*******************************************************************************
********************
**NGR
   8
*Card 8.1
```

```
** NRRD   NSRD    NC  NRTB  NRAD  NLTY  NSTA   NXF  NCAN  RADF    W3
NDM12 NDM13 NDM14
   25     0     1     1     0     0     1     1     0     0     0     0     0     0
*Card 8.2
**   N   IFTY   IAXP   NRND DAXMIN  RMULT      HGAP  ISECR  HTAMB   TAMB
*Card 8.3
**NSCH   PIE  NSCH   PIE  NSCH   PIE  NSCH   PIE  NSCH   PIE  NSCH   PIE  NSCH
PIE NSCH   PIE
    1     1     1     0     0  1.000 0.56783E+04     1  0.000  0.000
   1 0.250    2 0.250    7 0.250    8 0.250    0 0.000    0 0.000    0 0.000    0 0.000
    2     1     1     0     0  1.000 0.56783E+04     1  0.000  0.000
   2 0.250    3 0.250    8 0.250    9 0.250    0 0.000    0 0.000    0 0.000    0 0.000
    3     1     1     0     0  1.000 0.56783E+04     1  0.000  0.000
   3 0.250    4 0.250    9 0.250   10 0.250    0 0.000    0 0.000    0 0.000    0 0.000
    4     1     1     0     0  1.000 0.56783E+04     1  0.000  0.000
   4 0.250    5 0.250   10 0.250   11 0.250    0 0.000    0 0.000    0 0.000    0 0.000
    5     1     1     0     0  1.000 0.56783E+04     1  0.000  0.000
   5 0.250    6 0.250   11 0.250   12 0.250    0 0.000    0 0.000    0 0.000    0 0.000
    6     1     1     0     0  1.000 0.56783E+04     1  0.000  0.000

 7 0.250    8 0.250   13 0.250   14 0.250    0 0.000    0 0.000    0 0.000    0 0.000
    7     1     1     0     0  1.000 0.56783E+04     1  0.000  0.000
   8 0.250    9 0.250   14 0.250   15 0.250    0 0.000    0 0.000    0 0.000    0 0.000
    8     1     1     0     0  1.000 0.56783E+04     1  0.000  0.000
   9 0.250   10 0.250   15 0.250   16 0.250    0 0.000    0 0.000    0 0.000    0 0.000
    9     1     1     0     0  1.000 0.56783E+04     1  0.000  0.000
  10 0.250   11 0.250   16 0.250   17 0.250    0 0.000    0 0.000    0 0.000    0 0.000
   10     1     1     0     0  1.000 0.56783E+04     1  0.000  0.000
  11 0.250   12 0.250   17 0.250   18 0.250    0 0.000    0 0.000    0 0.000    0 0.000
   11     1     1     0     0  1.000 0.56783E+04     1  0.000  0.000
  13 0.250   14 0.250   19 0.250   20 0.250    0 0.000    0 0.000    0 0.000    0 0.000
   12     1     1     0     0  1.000 0.56783E+04     1  0.000  0.000
  14 0.250   15 0.250   20 0.250   21 0.250    0 0.000    0 0.000    0 0.000    0 0.000
   13     1     1     0     0  1.000 0.56783E+04     1  0.000  0.000
  15 0.250   16 0.250   21 0.250   22 0.250    0 0.000    0 0.000    0 0.000    0 0.000
   14     1     1     0     0  1.000 0.56783E+04     1  0.000  0.000
  16 0.250   17 0.250   22 0.250   23 0.250    0 0.000    0 0.000    0 0.000    0 0.000
   15     1     1     0     0  1.000 0.56783E+04     1  0.000  0.000
  17 0.250   18 0.250   23 0.250   24 0.250    0 0.000    0 0.000    0 0.000    0 0.000
   16     1     1     0     0  1.000 0.56783E+04     1  0.000  0.000
  19 0.250   20 0.250   25 0.250   26 0.250    0 0.000    0 0.000    0 0.000    0 0.000
   17     1     1     0     0  1.000 0.56783E+04     1  0.000  0.000
  20 0.250   21 0.250   26 0.250   27 0.250    0 0.000    0 0.000    0 0.000    0 0.000
```

```
   18     1     1     0     0  1.000 0.56783E+04     1  0.000  0.000
  21 0.250   22 0.250   27 0.250   28 0.250    0 0.000    0 0.000    0 0.000    0 0.000
   19     1     1     0     0  1.000 0.56783E+04     1  0.000  0.000
  22 0.250   23 0.250   28 0.250   29 0.250    0 0.000    0 0.000    0 0.000    0 0.000
   20     1     1     0     0  1.000 0.56783E+04     1  0.000  0.000
  23 0.250   24 0.250   29 0.250   30 0.250    0 0.000    0 0.000    0 0.000    0 0.000
   21     1     1     0     0  1.000 0.56783E+04     1  0.000  0.000
  25 0.250   26 0.250   31 0.250   32 0.250    0 0.000    0 0.000    0 0.000    0 0.000
   22     1     1     0     0  1.000 0.56783E+04     1  0.000  0.000
  26 0.250   27 0.250   32 0.250   33 0.250    0 0.000    0 0.000    0 0.000    0 0.000
   23     1     1     0     0  1.000 0.56783E+04     1  0.000  0.000
  27 0.250   28 0.250   33 0.250   34 0.250    0 0.000    0 0.000    0 0.000    0 0.000
   24     1     1     0     0  1.000 0.56783E+04     1  0.000  0.000
  28 0.250   29 0.250   34 0.250   35 0.250    0 0.000    0 0.000    0 0.000    0 0.000
   25     1     1     0     0  1.000 0.56783E+04     1  0.000  0.000
  29 0.250   30 0.250   35 0.250   36 0.250    0 0.000    0 0.000    0 0.000    0 0.000
*Card 8.6
**    I  NRT1   NST1   NRX1
     1    25      0      2
*Card 8.7
**IRTB1  IRTB2  IRTB3  IRTB4  IRTB5  IRTB6  IRTB7  IRTB8  IRTB9 IRTB10 IRTB11

IRTB12
     1     2     3     4     5     6     7     8     9    10    11    12
    13    14    15    16    17    18    19    20    21    22    23    24
    25
*Card 8.9
**    AXIALT      TRINIT
 0.00000E+00 0.25000E+03
 0.21336E+01 0.25000E+03
**********************************************************************
**********
*GROUP 9 - Conductor Geometry Description                             *
**********************************************************************
**********
**NGR
   9
*Card 9.1
** NFLT IRLF ICNF IMWR NDM5 NDM6 NDM7 NDM8 NDM9 NM10 NM11 NM12
NM13 NM14
     1    0    0    0    0    0    0    0    0    0    0    0    0    0
*Card 9.2
**  I FTYP       DROD       DFUL  NFUL IMTF IMTC IMOX DCRE      TCLD  FTDS IGPC
```

```
IGFC IRDP
   1 nucl 0.1118E-01 0.8890E-02     5    0    0    0 0.00 0.254E-03 0.95    0    0    0
*****************************************************************************
*********************
*GROUP 11 - Core Power Distribution Information                                *
*****************************************************************************
*********************
**NGR
  11
*Card 11.1
** NQA  NAXP  MNXN    NQ NGPFF   NQR  NDM7  NDM8  NDM9 NDM10 NDM11
NDM12 NDM13 NDM14
    1    1    4    0    0    1    0    0    0    0    0    0    0    0
*Card 11.2
** YQA
 0.00
*Card 11.3
**   I  NAXN
    1     4
*Card 11.4
**        Y      AXIALZ
 0.00000000  0.00000000
 0.00110000  1.00000000

 2.13250000  1.00000000
 2.13360000  0.00000000
*Card 11.7
** YQR
 0.00
*Card 11.8
**    FQR1      FQR2      FQR3      FQR4      FQR5      FQR6      FQR7      FQR8
 0.8260000 0.9890000 1.0260000 1.0480000 0.8270000 1.0550000 0.9840000 1.0250000
 0.9810000 1.0580000 1.0600000 1.0300000 1.2010000 1.0310000 1.0470000 1.0540000
 0.9970000 1.0300000 0.9830000 1.0450000 0.8340000 0.9930000 0.9940000 1.0550000
 0.8260000
*****************************************************************************
*********************
*GROUP 12 - Turbulent Mixing and Void Drift Data
*****************************************************************************
*********************
**NGR
  12
*Card 12.2
```

```
**    AAAK      DROD     THETM
 0.000E+01 0.1118E-01 0.500E+01
**********************************************************************************
********************
*GROUP 13 -  Boundary Condition Data                                              *
**********************************************************************************
********************
**NGR
  13
*Card 13.1
** NBND   NKBD NFUN NGBD NDM5 NDM6 NDM7 NDM8 NDM9 NM10 NM11
NM12 NM13 NM14
    72     0   0    0    0    0    0    0    0    0    0    0    0    0
*Card 13.4
**Inlet b.c. ------------------------------------------------------------
** IBD1   IBD2 ISPC N1FN N2FN N3FN    BCVALUE1    BCVALUE2    BCVALUE3
INITGAS
     1     1    2    0    0    0 0.00000E+00 0.13123E+04 0.00000E+00       1
     2     1    2    0    0    0 0.00000E+00 0.13123E+04 0.00000E+00       1
     3     1    2    0    0    0 0.00000E+00 0.13123E+04 0.00000E+00       1
     4     1    2    0    0    0 0.00000E+00 0.13123E+04 0.00000E+00       1
     5     1    2    0    0    0 0.00000E+00 0.13123E+04 0.00000E+00       1
     6     1    2    0    0    0 0.00000E+00 0.13123E+04 0.00000E+00       1
     7     1    2    0    0    0 0.00000E+00 0.13123E+04 0.00000E+00       1
     8     1    2    0    0    0 0.00000E+00 0.13123E+04 0.00000E+00       1

     9     1    2    0    0    0 0.00000E+00 0.13123E+04 0.00000E+00       1
    10     1    2    0    0    0 0.00000E+00 0.13123E+04 0.00000E+00       1
    11     1    2    0    0    0 0.00000E+00 0.13123E+04 0.00000E+00       1
    12     1    2    0    0    0 0.00000E+00 0.13123E+04 0.00000E+00       1
    13     1    2    0    0    0 0.00000E+00 0.13123E+04 0.00000E+00       1
    14     1    2    0    0    0 0.00000E+00 0.13123E+04 0.00000E+00       1
    15     1    2    0    0    0 0.00000E+00 0.13123E+04 0.00000E+00       1
    16     1    2    0    0    0 0.00000E+00 0.13123E+04 0.00000E+00       1
    17     1    2    0    0    0 0.00000E+00 0.13123E+04 0.00000E+00       1
    18     1    2    0    0    0 0.00000E+00 0.13123E+04 0.00000E+00       1
    19     1    2    0    0    0 0.00000E+00 0.13123E+04 0.00000E+00       1
    20     1    2    0    0    0 0.00000E+00 0.13123E+04 0.00000E+00       1
    21     1    2    0    0    0 0.00000E+00 0.13123E+04 0.00000E+00       1
    22     1    2    0    0    0 0.00000E+00 0.13123E+04 0.00000E+00       1
    23     1    2    0    0    0 0.00000E+00 0.13123E+04 0.00000E+00       1
    24     1    2    0    0    0 0.00000E+00 0.13123E+04 0.00000E+00       1
    25     1    2    0    0    0 0.00000E+00 0.13123E+04 0.00000E+00       1
```

```
   26    1   2   0   0   0 0.00000E+00 0.13123E+04 0.00000E+00      1
   27    1   2   0   0   0 0.00000E+00 0.13123E+04 0.00000E+00      1
   28    1   2   0   0   0 0.00000E+00 0.13123E+04 0.00000E+00      1
   29    1   2   0   0   0 0.00000E+00 0.13123E+04 0.00000E+00      1
   30    1   2   0   0   0 0.00000E+00 0.13123E+04 0.00000E+00      1
   31    1   2   0   0   0 0.00000E+00 0.13123E+04 0.00000E+00      1
   32    1   2   0   0   0 0.00000E+00 0.13123E+04 0.00000E+00      1
   33    1   2   0   0   0 0.00000E+00 0.13123E+04 0.00000E+00      1
   34    1   2   0   0   0 0.00000E+00 0.13123E+04 0.00000E+00      1
   35    1   2   0   0   0 0.00000E+00 0.13123E+04 0.00000E+00      1
   36    1   2   0   0   0 0.00000E+00 0.13123E+04 0.00000E+00      1
**outlet b.c. ------------------------------------------------------------
    1   22   1   0   0   0 0.00000E+00 0.16005E+04 0.15488E+03      1
    2   22   1   0   0   0 0.00000E+00 0.16005E+04 0.15488E+03      1
    3   22   1   0   0   0 0.00000E+00 0.16005E+04 0.15488E+03      1
    4   22   1   0   0   0 0.00000E+00 0.16005E+04 0.15488E+03      1
    5   22   1   0   0   0 0.00000E+00 0.16005E+04 0.15488E+03      1
    6   22   1   0   0   0 0.00000E+00 0.16005E+04 0.15488E+03      1
    7   22   1   0   0   0 0.00000E+00 0.16005E+04 0.15488E+03      1
    8   22   1   0   0   0 0.00000E+00 0.16005E+04 0.15488E+03      1
    9   22   1   0   0   0 0.00000E+00 0.16005E+04 0.15488E+03      1
   10   22   1   0   0   0 0.00000E+00 0.16005E+04 0.15488E+03      1
   11   22   1   0   0   0 0.00000E+00 0.16005E+04 0.15488E+03      1
   12   22   1   0   0   0 0.00000E+00 0.16005E+04 0.15488E+03      1
   13   22   1   0   0   0 0.00000E+00 0.16005E+04 0.15488E+03      1
   14   22   1   0   0   0 0.00000E+00 0.16005E+04 0.15488E+03      1
   15   22   1   0   0   0 0.00000E+00 0.16005E+04 0.15488E+03      1

   16   22   1   0   0   0 0.00000E+00 0.16005E+04 0.15488E+03      1
   17   22   1   0   0   0 0.00000E+00 0.16005E+04 0.15488E+03      1
   18   22   1   0   0   0 0.00000E+00 0.16005E+04 0.15488E+03      1
   19   22   1   0   0   0 0.00000E+00 0.16005E+04 0.15488E+03      1
   20   22   1   0   0   0 0.00000E+00 0.16005E+04 0.15488E+03      1
   21   22   1   0   0   0 0.00000E+00 0.16005E+04 0.15488E+03      1
   22   22   1   0   0   0 0.00000E+00 0.16005E+04 0.15488E+03      1
   23   22   1   0   0   0 0.00000E+00 0.16005E+04 0.15488E+03      1
   24   22   1   0   0   0 0.00000E+00 0.16005E+04 0.15488E+03      1
   25   22   1   0   0   0 0.00000E+00 0.16005E+04 0.15488E+03      1
   26   22   1   0   0   0 0.00000E+00 0.16005E+04 0.15488E+03      1
   27   22   1   0   0   0 0.00000E+00 0.16005E+04 0.15488E+03      1
   28   22   1   0   0   0 0.00000E+00 0.16005E+04 0.15488E+03      1
   29   22   1   0   0   0 0.00000E+00 0.16005E+04 0.15488E+03      1
   30   22   1   0   0   0 0.00000E+00 0.16005E+04 0.15488E+03      1
```

```
   31    22   1   0   0   0 0.00000E+00 0.16005E+04 0.15488E+03      1
   32    22   1   0   0   0 0.00000E+00 0.16005E+04 0.15488E+03      1
   33    22   1   0   0   0 0.00000E+00 0.16005E+04 0.15488E+03      1
   34    22   1   0   0   0 0.00000E+00 0.16005E+04 0.15488E+03      1
   35    22   1   0   0   0 0.00000E+00 0.16005E+04 0.15488E+03      1
   36    22   1   0   0   0 0.00000E+00 0.16005E+04 0.15488E+03      1
*******************************************************************************
**********************
*GROUP 14 - Output Options
*******************************************************************************
**********************
**NGR
  14
*Card 14.4
** N1 NOU1 NOU2 NOU3 NOU4 IPRP IOPT IITY DNB IMASS IHEAT ICHAN
IGAP KRY
   5   0   0   0   0   0   0   1   0   1   1   1   1   0
*******************************************************************************
**********************
*GROUP 15 - Time Domain Data
*******************************************************************************
**********************
**NGR
  15
*Card 15.1
**   DTMIN      DTMAX      TEND       EDINT      DMPINT     RTWFP    MAXITS
 0.1000E-05 0.1000E-01 0.1000E+00 0.0000E+00 0.0000E+00 0.1000E+04     10000
-0.1000E+01 0.0000E+00 0.0000E+00 0.0000E+00 0.0000E+00 0.0000E+00
```